Monthly Notices of the ROYAL ASTRONOMICAL SOCIETY

MNRAS **528,** 3531–3548 (2024) https://doi.org/10.1093/mnras/stae251
Advance Access publication 2024 January 24

On an apparent dearth of recurrent nova super-remnants in the Local Group

M. W. Healy-Kalesh [1]★ M. J. Darnley [1] and M. M. Shara [2]

[1]*Astrophysics Research Institute, Liverpool John Moores University, IC2 Liverpool Science Park, Liverpool L3 5RF, UK*
[2]*Department of Astrophysics, American Museum of Natural History, Central Park West at 79th Street, New York, NY 10024, USA*

Accepted 2024 January 9. Received 2024 January 8; in original form 2023 November 20

ABSTRACT

The Andromeda Galaxy is home to the annually erupting recurrent nova (RN) M 31N 2008-12a (12a); the first nova found to host a nova super-remnant (NSR). An NSR is an immense structure surrounding a RN, created from many millions of eruptions sweeping up material in the local environment to form a shell tens of parsecs across. Theory has demonstrated that NSRs should be found around all recurrent novae (RNe), even those systems with long periods between eruptions. Befittingly, the second NSR was found around the Galactic classical (and long suspected recurrent) nova, KT Eridani. In this Paper, we aim to find more of these phenomena through conducting the first ever survey for NSRs in M 31 and the Large Magellanic Cloud (LMC). We find that the surroundings of fourteen RNe in M 31 as well as the surroundings of the four RNe in the LMC do not show any evidence of vast parsec-scale structures in narrow-band (H α and [S II]) images, unlike the one clearly seen around 12a, and therefore conclude that observable NSRs are either rare structures, or they are too faint (or small) to be detected in our existing data sets. Yet, the NSR surrounding 12a would also likely to have been overlooked in our study if it were approximately one magnitude fainter. Searches for NSRs around other RNe 'masquerading' as classical novae may prove to be fruitful as would whole surveys of other Local Group galaxies.

Key words: novae, cataclysmic variables – ISM: general.

1 INTRODUCTION

Nova eruptions rank among some of the most luminous stellar transients. At their heart is a white dwarf (WD), accreting hydrogen-rich material from a donor within a close binary configuration (Warner 1995). Once a critical mass has accumulated on the WD surface, a thermonuclear runaway ensues that ejects a proportion of the accreted material (Starrfield et al. 1972; Prialnik, Shara & Shaviv 1978) – this is the nova eruption itself and it is associated with a substantial increase in the luminosity of the system.

Nova eruptions are inherently recurrent and systems are commonly classified by virtue of their observed inter-eruption cycle. The classical novae (CNe) are those systems with long recurrence periods $P_{\rm rec}$, whereas the recurrent novae (RNe) have undergone at least two observed eruptions. Here, there are clear selection effects that limit the known recurrent nova (RN) population, with many recurrents 'masquerading' as their classical siblings (Pagnotta & Schaefer 2014). As an example, the Galactic classical nova (CN) KT Eridani has been observed only once in eruption (in 2009) however, after detailed analysis of system's characteristics, Schaefer et al. (2022) conclude that KT Eridani is an RN with a $P_{\rm rec}$ of 40–50 yr (as do Shara et al. 2023 and Healy-Kalesh et al. 2023b).

Recurrence period is primarily a function of the WD mass and the mass accretion rate ($\dot{M}$). The combination of a high-mass WD and high $\dot{M}$ is required to drive $P_{\rm rec}$ below, of order, a century (see e.g. Yaron et al. 2005) to move a nova into the position of potentially being classed as an RN (see discussion within Darnley 2021). Such a high-mass WD and likelihood to grow more massive due to the retention of accumulated material (see e.g. Yaron et al. 2005; Hillman et al. 2015, 2016; Kato, Saio & Hachisu 2015); place RNe among the front-runners for progenitors of Type Ia supernovae (SNe Ia; Whelan & Iben 1973; Hachisu et al. 1999a; Hachisu, Kato & Nomoto 1999b; Hillebrandt & Niemeyer 2000).

Every nova eruption ejects high-velocity material into the surrounding interstellar medium (ISM). This is well evidenced through the recovery of numerous remnants from single nova eruptions such as those around Z Camelopardalis (Shara et al. 2007), GK Persei (Bode, O'Brien & Simpson 2004; Harvey et al. 2016), AT Cancri (Shara et al. 2012), DQ Herculis (Williams et al. 1978), HR Delphini (Harman & O'Brien 2003), DO Aquilae, and V4362 Sagittarii (Harvey et al. 2020). With recurrence periods for most of the known CNe being longer than 1 kyr, perhaps up to 1 Myr, many remnants will have essentially dissipated before the subsequent eruption takes place (Healy-Kalesh et al. 2023a).

However, for RNe, this is not the case. Here, the inter-eruption time-scales are short enough ($P_{\rm rec} < 100$ yr), that the *next* eruption will occur while the previous ejecta maintain a substantial over-density and before they have had time to cool. A striking example of interacting ejecta from a handful of recent eruptions surrounds the Galactic RN T Pyxidis, in the form of over two thousand [N II]-emitting knots (Shara et al. 1997, 2015). The knots (and

★ E-mail: m.w.healykalesh@ljmu.ac.uk

filaments) surrounding T Pyxidis are a consequence of Rayleigh–Taylor instabilities brought about by the interaction of six RN ejecta shells with a proposed CN shell (Toraskar et al. 2013; Shara et al. 2015). Three-dimensional simulations mimicking this history (Toraskar et al. 2013) supports the Schaefer, Pagnotta & Shara (2010) hypothesis that T Pyxidis experienced a CN eruption in 1866 after millennia of hibernation, and followed this up with six RN eruptions driven by a period of elevated mass-loss from the donor that is a proposed consequence of the CN eruption. We note that the T Pyxidis scenario is not expected to be typical of RNe.

The Andromeda Galaxy (M 31) RN M31N 2008-12a (hereafter simply '12a') exhibits the shortest recurrence period currently known: $P_{\rm rec} = 359 \pm 12$ d (Darnley et al. 2014, 2016). The eruptions from 12a are powered by a near-Chandrasekhar mass ($M_{\rm WD} \simeq 1.38\,{\rm M}_{\odot}$; Kato, Saio & Hachisu 2015) WD accreting at $1.6 \times 10^{-7} \lesssim \dot{M} \lesssim 1.4 \times 10^{-6}\,{\rm M}_{\odot}\,{\rm yr}^{-1}$ (Darnley et al. 2017) – both paramaters are at the extreme high end of values seen in other novae. Darnley et al. (2015) reported the discovery of a vast shell-like nebula surrounding 12a, measuring 134 pc across at its largest extent. Supported by hydrodynamic simulations of 10^5 12a-like eruptions, Darnley et al. (2019) proposed that this nebula was the result of $\sim 6 \times 10^6$ eruptions as the 12a WD has grown (over $\sim 6 \times 10^6$ yr) toward the Chandrasekhar mass – producing the first discovered nova super-remnant (NSR).

Subsequent, and more detailed, hydrodynamic modelling by Healy-Kalesh et al. (2023a) has shown that vast dynamical NSRs should exist around all RNe, including those systems with shrinking WDs or with eruptions thousands of years apart. In addition, Healy-Kalesh et al. (2023a) demonstrated that the size of an NSR depends strongly upon $\dot{M}$, the surrounding ISM density, and the observed $P_{\rm rec}$ (i.e. the instantaneous WD mass) whereas WD temperature and initial mass have less of an impact. Though, if the initial mass is very high, indicative of an oxygen–neon (ONe) WD, the extent of the grown NSR is largely reduced. Yet, it is only systems with high-accretion rates that are predicted to have *observable* NSRs (Healy-Kalesh et al. 2023a). Furthermore, as the population of novae surrounded by an NSR likely host a high-mass WD, possibly close to the Chandrasekhar limit, then these vast structures may represent indicators for the locations of upcoming or past SNe Ia events (Darnley 2021). As such, NSRs may help explore the SN Ia population that has taken the single degenerate (nova) pathway.

As predicted by Healy-Kalesh et al. (2023a), the on-sky size of any Galactic NSRs would be prohibitively large for facilities with small field of views. Indeed, attempts so far to find evidence of associated NSRs around a number of Galactic RNe using conventional small mid-sized facilities has proved futile; this is not surprising as these NSRs will have the same (very low, if not lower) surface brightness as the 12a NSR but cover a much larger proportion of the sky. Significantly though, the 2.3×1.5 square degrees field of view and dedicated observing campaign with the new Condor Array Telescope (Lanzetta et al. 2023) has led to the discovery of a new NSR: a 50 pc shell surrounding the Galactic nova, KT Eridani, thereby likely confirming its RN status (Shara et al. 2023; Healy-Kalesh et al. 2023b).

M 31 is the leading laboratory to study nova population statistics (Shafter 2019; Darnley & Henze 2020), due to its high nova rate (Darnley et al. 2006), the uniform, yet close, distance to all novae and the low absorbing column in that direction. Additionally, in M 31 and the sufficiently distant Large Magellanic Cloud (LMC), NSRs should be of order a few tens of arcseconds across unlike their Galactic counterparts that span many degrees on the sky. As such, M 31 and the LMC may provide ideal sites to search for NSRs; this is the motivation for the following work.

In this paper, we present both the results of a targeted search within the LMC and a survey within M 31 specifically searching for NSRs. In Section 2, we outline the data used in this work and follow this with our analysis of the surroundings of each recurrent nova in Section 3. We present of results of this analysis in Section 4 and discuss implications in Section 5, before concluding our paper in Section 6.

2 OBSERVATIONS AND SIMULATIONS

2.1 M31N 2008–12a nova super-remnant

Prior to the discovery of 12a (by Nishiyama & Kabashima 2008) and the subsequent realization of its recurrent nature, its surrounding NSR had already been serendipidously captured by several wide-field surveys (see e.g. Walterbos & Braun 1992; Azimlu, Marciniak & Barmby 2011). However, its potential association with 12a only became apparent following the 2014 eruption (see Darnley et al. 2015, 2019, and references therein). The 12a NSR was clearly visible in ground-based narrow-band Hα and [S II] λ6713, 6731 imaging data (but not [O III] λ5007, due to a lack of such emission) collected as part of the Local Group Galaxies Survey (LGGS; Massey et al. 2006, 2007). Fig. 1 presents LGGS data in the immediate vicinity of 12a and reveals the extended nebulosity in Hα and [S II] around the system; the LGGS [O III] and a deeper Liverpool Telescope Hα image are also provided.

2.2 Local Group Galaxy Survey data and image processing

At the time of writing, there are 20 known RNe in M 31 (see Table 1). The majority were recovered through work by Shafter et al. (2015), with M31N 2017–01e confirmed by Williams & Darnley (2017), M31N 1923–12c by Darnley & Williams (2021), and M31N 2013–10c by Shafter et al. (2023).

The positions of all 20 RNe are well covered by at least one field of the LGGS survey, with 13 appearing in two of the ten fields, and five in three fields. In Fig. 2, we show the approximate placing of the ten LGGS fields and the positions of all 20 known RNe. In this study we utilize the narrow-band Hα, [S II] and [O III] and broad-band V and R imaging data from LGGS. The LGGS processed science data (see Massey et al. 2006, 2007) were obtained from the Lowell web pages.[1]

Continuum subtraction of the LGGS images was performed using IRAF (Tody 1986, 1993) following matching photometry with DAOPHOT (Stetson 1987) between suitable narrow- and broad-band pairs: R for Hα and [S II]; V for [O III]. As described in Section 3, narrow-band fluxes, per square-arcsecond, for Hα and [S II] were computed following the methodology presented in Schaefer (2010). The projected distance from the source is computed assuming an M31 distance of 778 kpc (Stanek & Garnavich 1998). Fig. A1 illustrates the results of this image processing for 12a where the Hα and [S II] subtracted images show a clear broad emission structure, compared to the [O III] image. In the same manner, we illustrate the results of the continuum subtraction for the LGGS Hα, [S II], and [O III] images surrounding the other 19 RNe in Figs A2–A19.

[1] http://www.lowell.edu/users/massey/lgsurvey given in Massey et al. (2006).

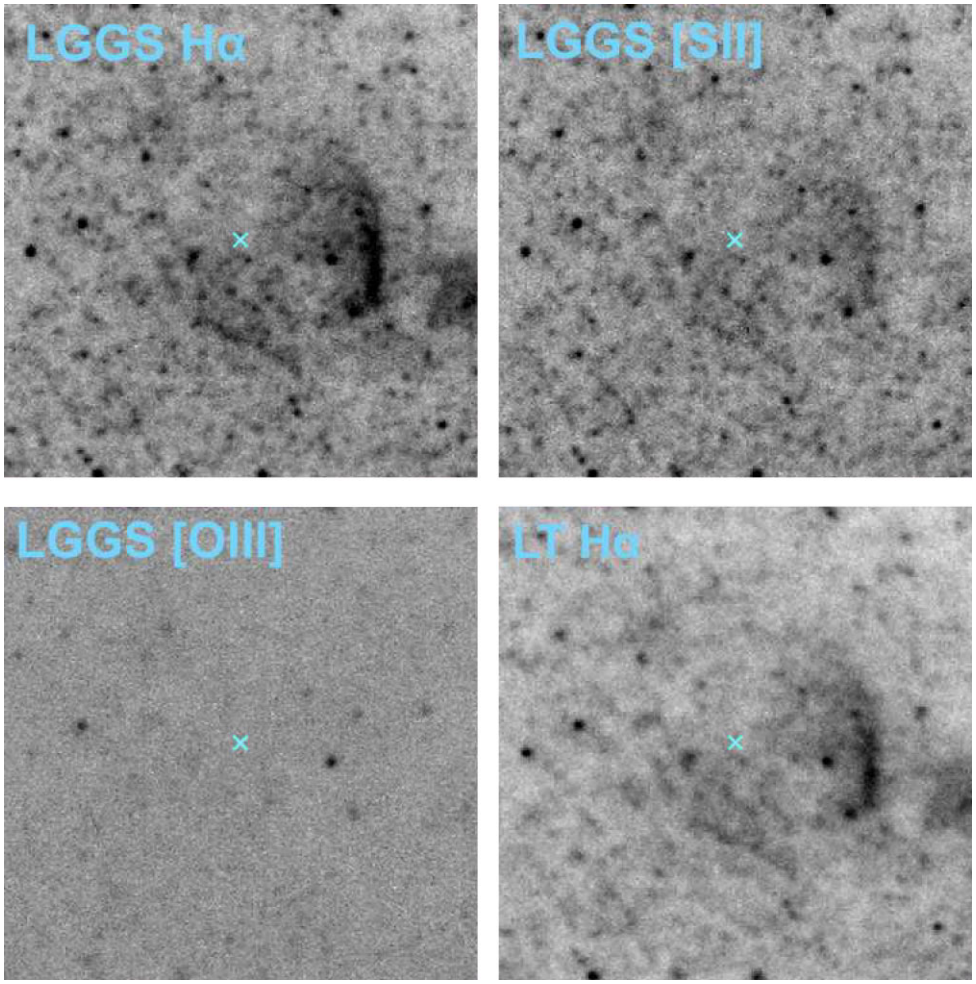

Figure 1. Local Group Galaxies Survey (LGGS; Massey et al. 2007) narrow-band imaging (from field 2) of the 1 arcmin × 1 arcmin region surrounding M31N 2008-12a. Top-left: LGGS H α. Top-right: LGGS [S II]. Bottom-right: LGGS [O III]. Bottom-left: Liverpool Telescope deeper H α image.

2.3 Faulkes Telescope South data and image processing

In the Large Magellanic Cloud, there are four known RNe (see Table 1) – we show their locations in Fig. 3. As for the potential NSRs in M 31, the NSRs surrounding each of the RNe in the LMC will subtend a small enough angular size[2] to be observed within one field of view of many ground-based telescopes.

As such, we observed the surroundings of each of the four RNe in the LMC with the Faulkes Telescope South (FTS)[3] as any existing NSRs will fit comfortably within the 10.5 arcmin × 10.5 arcmin field of view of the Spectral Imager camera on this 2-m telescope. We utilized narrow-band H α and [O III] and broad-band R and V filters on FTS (see Table 2 for details of these data): the H α imaging to detect emission from an NSR shell; the [O III] imaging to rule out the possibility of any identified remnants having a different origin (for example see Section 4.2.3) and the R and V imaging for continuum subtraction.

We performed continuum subtraction using the same method as with the M 31 LGGS data using IRAF (Tody 1986, 1993) and DAOPHOT (Stetson 1987). As described in Section 3, narrow-band fluxes, per square-arcsecond, were then computed in the same manner as for the LGGS data following the methodology presented in Schaefer (2010) and the projected distance from the source is computed assuming a distance to the LMC of 49.59 kpc (Pietrzyński et al. 2019). We show the results of this image processing for the FTS H α and [O III] images surrounding the four RNe in Figs A20–A23.

2.4 Predicted NSR H α luminosity from simulations

The simulations presented in Healy-Kalesh et al. (2023a) replicate the evolution of a range of nova systems and the subsequent creation of each system's NSR. One of these simulations was utilized to model the H α emission from a remnant forming around a 1×10^7 K WD with an accretion rate of $1 \times 10^{-7}\,M_\odot\,yr^{-1}$ as it grew from $1\,M_\odot$ to the Chandrasekhar limit (see Healy-Kalesh et al. 2023a, their fig. 14). We reproduce a version of this figure here converted to illustrate H α luminosity evolution in Fig. 4 for such a system located within an ISM of $1.67 \times 10^{-24}\,g\,cm^{-3}$ (1 H atom cm^{-3}), which we will denote as $n = 1$ (cyan line), along with the evolution of H α emission from the same system placed within different environments: $1.67 \times 10^{-25}\,g\,cm^{-3}$ ($n = 0.1$, blue), $1.67 \times 10^{-23}\,g\,cm^{-3}$ ($n = 10$, green), and $1.67 \times 10^{-22}\,g\,cm^{-3}$ ($n = 100$, red). We have displayed the 20 RNe in Fig. 4 using their respective recurrence periods to estimate the H α luminosity from each system. By inspection, the

[2]Angular radii of 1.4, 1.0, 0.8, and 0.4 arcmin for LMCN 1968–12a, LMCN 1996, LMCN 1971–08a, and YY Doradus, respectively.
[3]ID number: NSF2022B-004.

Table 1. Details of the 20 known M 31 recurrent novae and four LMC recurrent novae. For M 31, we state the LGGS fields covering each nova with LGGS field numbers shown in parentheses indicating novae that are contained within an LGGS field, but are too close to an edge to allow sufficient remnant analysis. We also use modelling of H α emission from simulations of NSRs presented in Healy-Kalesh et al. (2023a) to predict the H α luminosity of each NSR (see Section 2.4 for details and Fig. 4).

Name	R.A. (J2000)	Decl. (J2000)	Eruptions	$P_{\rm rec}$ (yr)	LGGS field(s)	Predicted NSR H α luminosity (erg s^{-1})	References
M31N 2008–12a	00:45:28.80	+41:54:10.1	19	0.996 ± 0.030	2, 3	1.15×10^{33}	1, 2, 3
M31N 2017–01e	00:44:10.72	+41:54:22.1	4	2.545 ± 0.020	3	3.63×10^{32}	4, 5
M31N 1926–07c	00:42:53.37	+41:15:43.7	3	∼3	5, 6	3.62×10^{32}	6
M31N 1997–11k	00:42:39.59	+41:09:04.0	3	∼4	5, 6	2.63×10^{32}	1, 2
M31N 1963–09c	00:42:57.74	+41:08:12.1	4	∼5	5, 6, (7)	2.23×10^{32}	1, 2
M31N 1960–12a	00:42:55.66	+41:14:11.7	3	∼6	5, 6	1.90×10^{32}	1, 2
M31N 1984–07a	00:42:47.24	+41:16:19.8	3	∼8	(4), 5, 6	1.53×10^{32}	1, 2
M31N 2006–11c	00:41:33.17	+41:10:12.4	2	∼8	6	1.53×10^{32}	1, 2
M31N 1990–10a	00:43:04.05	+41:17:07.5	3	∼9	4, 5, 6	1.42×10^{32}	1, 2
M31N 2007–11f	00:41:31.52	+41:07:13.1	2	∼9	6, 7	1.42×10^{32}	1, 2
M31N 1923–12c	00:42:38.37	+41:08:45.8	2	∼9	5, 6, (7)	1.42×10^{32}	7
M31N 2013–10c	00:43:09.32	+41:15:41.6	2	∼10	5, 6	1.28×10^{32}	8, 9
M31N 2007–10b	00:43:29.50	+41:17:13.0	2	∼10	4, 5, 6	1.28×10^{32}	1, 2
M31N 1982–08b	00:46:06.60	+42:03:48.0	2	∼14	1, 2, 3	9.96×10^{31}	1, 2
M31N 1945–09c	00:41:28.55	+40:53:14.1	2	∼27	6, 7, 8	5.64×10^{31}	1, 2
M31N 1926–06a	00:41:41.00	+41:03:36.7	2	∼37	6, 7	4.15×10^{31}	1, 2
M31N 1966–09e	00:39:30.80	+40:29:15.0	2	∼41	8, 9	3.75×10^{31}	1, 2
M31N 1961–11a	00:42:31.43	+41:16:22.1	2	∼44	5, 6	3.46×10^{31}	1, 2
M31N 1953–09b	00:42:20.74	+41:16:14.1	2	∼51	5, 6	2.89×10^{31}	1, 2
M31N 1919–09a	00:43:28.76	+41:21:42.6	2	∼79	4, 5, 6	2.03×10^{31}	1, 2
LMCN 1968–12a	05:09:58.40	–71:39:52.7	4	6.2 ± 1.2	–	1.85×10^{32}	10
LMCN 1996	05:13:30.00	–68:38:00.0	2	∼22	–	6.89×10^{31}	11
LMCN 1971–08a	05:40:44.20	–66:40:11.6	2	∼38	–	4.04×10^{31}	12
YY Doradus	05:56:42.40	–68:54:34.5	2	∼67	–	2.22×10^{31}	13, 14

Notes. References – (1) Shafter et al. (2015), (2) Darnley (2021), (3) Sun et al. (2023), (4) Williams & Darnley (2017), (5) Shafter et al. (2022b), (6) Shafter et al. (2022a), (7) Darnley & Williams (2021), (8) Xu et al. (2023), (9) Shafter et al. (2023), (10) Kuin et al. (2020), (11) Mróz & Udalski (2018), (12) Bode et al. (2016), (13) Bond et al. (2004), and (14) Mason et al. (2004).

first peak of H α emission in the different environments occurs earlier as the ISM density is increased (∼6×10^3 yr for $n = 100$ compared to ∼8×10^5 for $n = 0.1$). However, after this initial peak, the NSR H α luminosity then follows a similar evolutionary trend for each of different ISM densities. Beyond this, the NSR located within the highest density ISM ($n = 100$) continues to be the brightest in H α, ending with $L_{\rm H\,\alpha} \simeq 8.6 \times 10^{33}$ erg s^{-1} compared $L_{\rm H\,\alpha} \simeq 5.7 \times 10^{32}$ erg s^{-1} in the $n = 0.1$ surroundings.

As a first-order approximation for the total H α luminosity from each potential NSR in M 31, we assumed an ISM density of 1.67×10^{-24} g cm^{-3} and computed the corresponding H α luminosity at the system's current recurrence period. The predicted total H α luminosity from an NSR for each of the 20 M 31 RNe and 4 LMC RNe are provided in Table 1.

The H α luminosity from the 12a NSR is larger than all other predicted NSRs (see Table 1) due to its higher mass WD and therefore longer evolution. It therefore experiences highly energetic eruptions at late times that travel through the already established NSR ejecta pile-up region before colliding with the formed high-density shell, leading to collisional excitation and high levels of recombination (Healy-Kalesh et al. 2023a). From this modelling, we conclude that 12a should have the NSR with the highest total H α luminosity out of the 20 RNe in M 31 and the four RNe in the LMC.

3 ANNULAR PHOTOMETRY

To search for excess, extended, emission around each RN, we perform annular photometry at the position of each M 31 nova in all of the LGGS fields in which they are found and for the LMC novae in each image, out to 295 arcsec in all frames.

The annular photometry consisted of 500 circular annuli (970 for FTS data) with radii logarithmically distributed from 0 to 135 arcsec (295 arcsec for FTS data). To remain consistent between different data sets, for both the LGGS data and the FTS data, we used the methodology provided in Schaefer (2010) and photometry from *Gaia* DR2 (Gaia Collaboration 2016, 2018) to convert the images from counts s^{-1} to flux per count in units of erg s^{-1} cm^{-2} Å^{-1}, before applying a scaling of the flux to account for differences between the $G_{\rm RP}$ filter (Gaia Collaboration 2018; Weiler 2018) and the LGGS H α filter and [S II] filter (Massey et al. 2007) and the FTS H α filter.[4] Additionally, we applied pixel masking to remove clear artefacts at large radii – the origins of which were bright stars coincident with the surroundings of the novae.

The results of our continuum-subtracted, pixel-masked H α and [S II] luminosity radial profiles for the M 31 data are shown in Figs 5 and 6, respectively. We have removed 1926–07c, 1960–12a, 1984–07a, 1990–10a, and 1961–11a from our analysis as they are all too close to the bulge of M 31 (see Fig. 7) to allow any form of sufficient data processing, after continuum subtraction, in the same manner as other regions of the galaxy. The equivalent for the H α luminosity radial profiles for the LMC data is shown in Fig. 8. We have not included the [O III] luminosity radial profiles for either the M 31 or LMC data as all profiles are very noisy and are consistent with zero excess flux for all RN, including 12a.

[4] https://lco.global/observatory/instruments/filters/

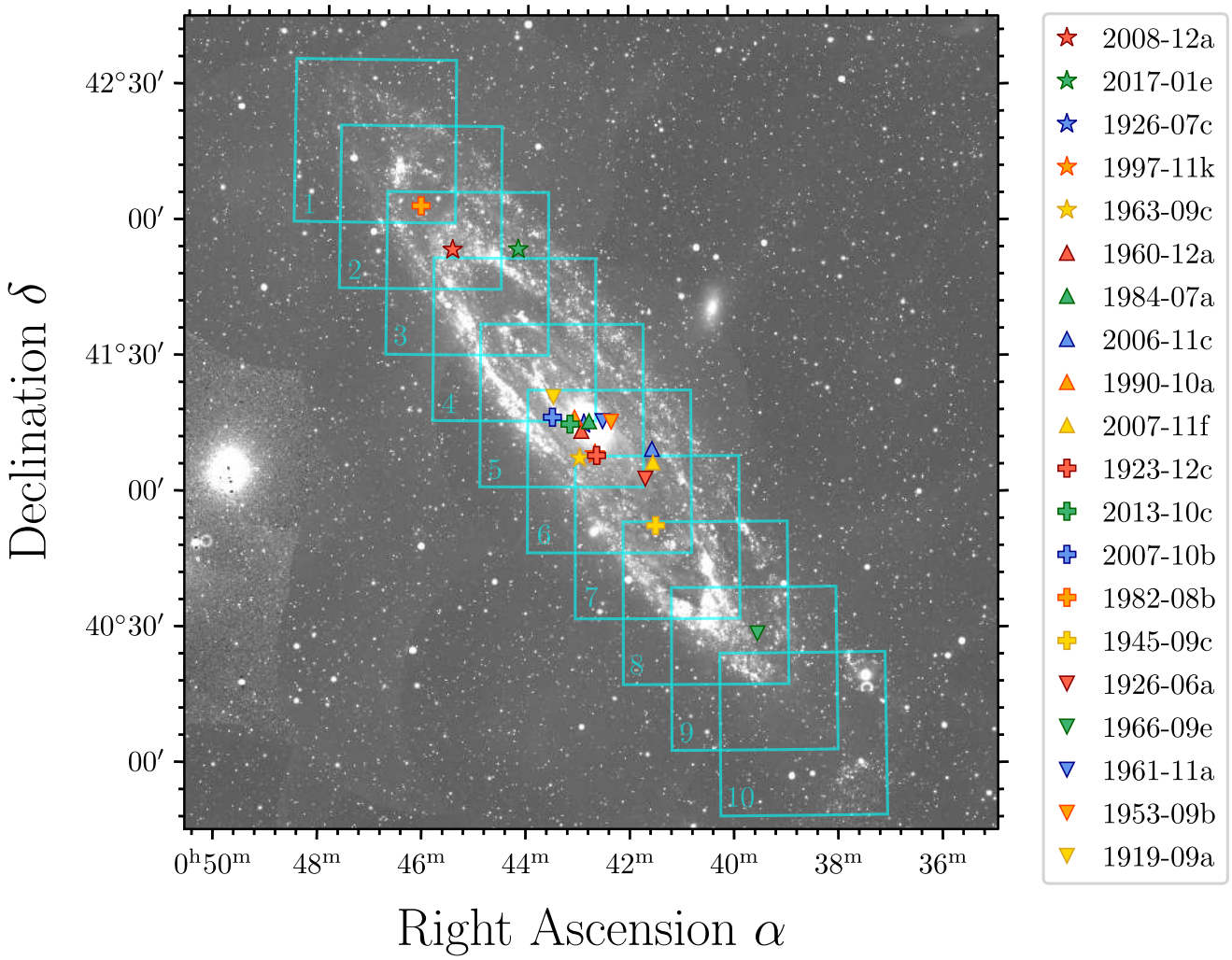

Figure 2. A near-ultraviolet (UV) 3° × 3° mosaic image of M 31 taken by Galaxy Evolution Explorer (GALEX).The approximate positions of the ten LGGS fields are overlaid in cyan squares and the positions of the 20 known M 31 recurrent novae are provided. In Fig. 7, we show the same near-UV GALEX image but zoomed-in on the bulge of M 31.

4 RESULTS

The aim of this survey of M 31 and targeted search within the LMC was to discover more NSRs to place alongside the NSRs around M 31N 2008–12a (Darnley et al. 2019; Healy-Kalesh et al. 2023a) and KT Eridani (Shara et al. 2023; Healy-Kalesh et al. 2023b). As the emission from the NSR around 12a can be clearly seen in 1 arcmin × 1 arcmin H α and [S II] LGGS images centred on the nova (shown in Fig. 1 and Fig. A1), we would also expect to see similar emission in the same vicinity of other RNe within M 31 and the LMC if they were to also host a *visible* NSR.

4.1 M31

We can clearly see by looking at the continuum subtracted narrow-band images in Figs A2–A19 that there is an absence of evidence for such emission around all other RNe in M 31. Furthermore, the results of annular photometry performed on the H α and [S II] LGGS images for each of the other RNe, as described in Section 3 and provided in Figs 5 and 6, respectively, quantify this lack of observable emission in comparison to 12a. For the five RNe that are too close to the bulge of M 31, we cannot speculate about whether these systems host an observable NSR.

4.1.1 H α luminosity

The characteristic shell surrounding M 31N 2008–12a is trivially recoverable in the H α LGGS image. This is reflected in Fig. 5, with the surplus of H α emission from the nova out to approximately 35 arcsec. At the distance of M 31, this is equivalent to ∼130 pc – consistent with the 12a NSR projected size of 134 pc (Darnley et al. 2019). The peak emission is approximately 1.6×10^{36} erg s^{-1} Å^{-1} arcsec^{-2} at ∼17 arcsec (projected size of ∼64 pc).

Clearly, the predicted H α emission of 12a from simulations as described in Section 2.4 (1.15×10^{33} erg s^{-1} in Table 1) does not match the total integrated H α luminosity from the LGGS observations (∼6×10^{37} erg s^{-1}). The discrepancy may arise from the models placing the NSR in an ISM with a much lower density than it is actually situated. From Fig. 4, we show that this has a large effect on the H α flux of an NSR. Other factors potentially playing a role in this discrepancy include the cooling package employed in the Healy-Kalesh et al. (2023a) simulations not being scaled for

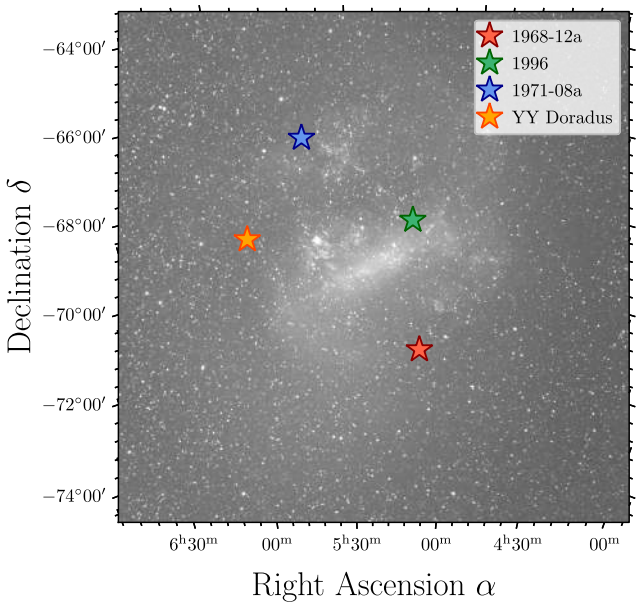

Figure 3. An optical 12° × 12° mosaic image of the LMC taken by Axel Mellinger (Mellinger 2009). The positions of the four known LMC recurrent novae are provided.

Table 2. Details of observations of the surroundings of the four RNe in the LMC with the Spectral Imager on the Faulkes Telescope South (exposure and number of exposures).

Name	H α	R band	[O III]	V band
LMCN 1968–12a	720s × 4	180s × 3	180s × 3	180s × 3
LMCN 1996	720s × 4	180s × 3	180s × 3	180s × 3
LMCN 1971–08a	720s × 3	180s × 3	180s × 3	180s × 3
YY Doradus	720s × 4	180s × 3	180s × 3	180s × 3

lower densities of ISM; assuming a pure-hydrogen ISM or assuming the ejecta and ISM are spherically symmetric (Healy-Kalesh et al. 2023b).

The other fourteen H α flux radial profiles shown in Fig. 5 resemble noise that is consistent with zero excess flux; we have provided a negative section of the y-axis to illustrate this. For example, 1923–12c looks to have a peak at ∼2–3 arcsec however, at radii <2 arcsec the flux drops below zero by approximately the same amount, indicative of noise. Moreover, by inspection, this peak is likely from an artefact created during continuum subtraction of a very nearby source. 1953–09b has a peak of $\sim 6 \times 10^{35}$ erg s^{-1} Å^{-1} arcsec^{-2} at ∼2 arcsec, but again, the flux either side of this region drops below zero by a similar factor.

Both 2017–01e and 1919–09a have small bumps at the lowest radius (between 1 and 2 arcsec) followed by a flat, albeit noisy, profile. However, as shown by the scaled point source function (PSF) for the H α LGGS data in Fig. 5, this initial peak in both profiles can be attributed to the PSF of the central object – which may indeed be the quiescent nova system, bright in H α due to accretion.

Potentially, some of the RNe without a structure may have a faint NSR only just below the detection limit of LGGS. If this was the case, then combining all of the surroundings centred on each RNe we analysed may reveal a faint glow out to approximately 30 arcsec. To test this we took the 1 arcmin × 1 arcmin surroundings of the fourteen M 31 RNe we analysed, aligned them by the location of the nova and then co-added the images. However, the fully combined image did not display excess emission.

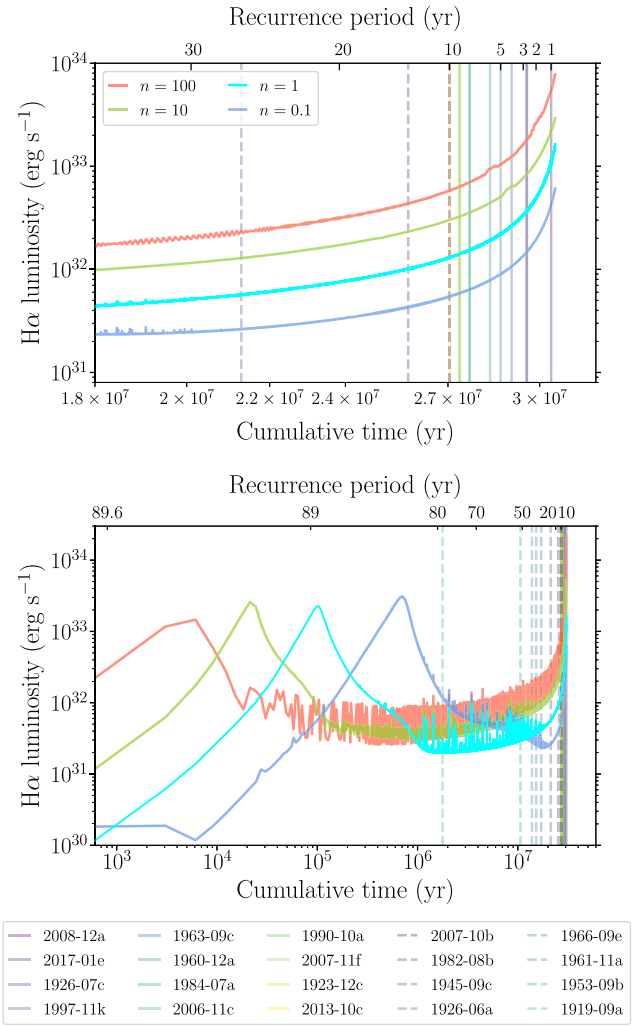

Figure 4. The evolution of NSR H α luminosity for the reference simulation ($n = 1$) and simulations with difference ISM densities; Run 2 ($n = 0.1$), Run 5 ($n = 10$), and Run 7 ($n = 100$) presented in Healy-Kalesh et al. (2023a). The bottom panel shows the NSR H α luminosity throughout the full evolution of the simulations up to $\sim 3.1 \times 10^7$ yr whereas the top panel focusses on a cumulative time of 1.8×10^7 yr for clarity. Also, to remove the impact of single eruptions, we re-bin to a lower temporal resolution in the *top panel*. The vertical lines indicate the recurrence periods of all 20 RNe in M 31 and their associated cumulative time from the NSR simulations in Healy-Kalesh et al. (2023a).

4.1.2 [S II] *luminosity*

As with the extended emission for 2008–12a derived from the LGGS H α data, we see a similarly extended profile of [S II] emission. As we would expect, this emission is fainter but is still able to quantify the NSR structure surrounding 12a. The extended emission reaches out to approximately 22 arcsec which is equivalent to a projected size of ∼83 pc. Whilst this does not match the furthest extent of the H α profile of 12a (see Section 4.1.1), it is likely that the faintness of the [S II] emission compared to H α contributes to the lack of detection at the outer regions.

The [S II] luminosity radial profiles for the other M 31 RNe somewhat mimic their H α counterparts. 1923–12c again has an evident peak between ∼2–3 arcsec but can be attributed to a similar continuum subtraction artefact of a nearby source and is consistent

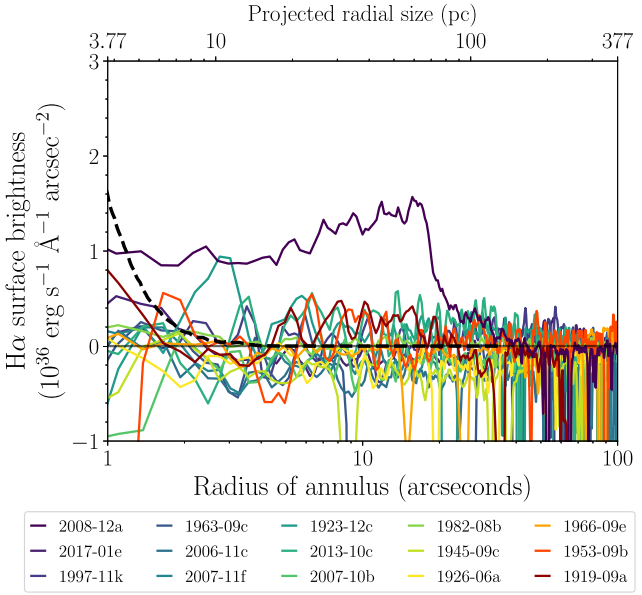

Figure 5. The Hα luminosity surface brightness of the surroundings of fiftee novae in M 31 out to 100 arcsec (with a projected size of ∼377 pc at a distance of M 31) – the luminosity for the other five novae were omitted as their close proximity to the bulge of M 31 prevented sufficient data processing in comparison to the other novae (see Fig. 7). This is emission determined from annular photometry after continuum subtraction and pixel masking of the bright sources in the images. We also show the PSF for the LGGS data (black dashed line).

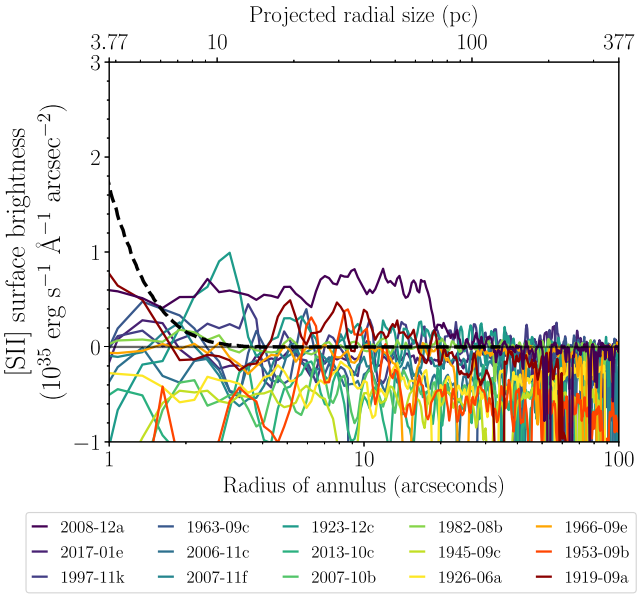

Figure 6. As in Fig. 5 but with the [S II] luminosity surface brightness surrounding each of the fifteen M 31 RN we analysed.

with noise. There is a bump near the origin (<3 arcsec) in the luminosity profile for 1963–09c but this fits with the scaled PSF for this data. Similarly, the surroundings of 1919–09a reveal a bump near the centre of the profile (<2 arcsec) that is consistent with the PSF of the image. Other than these peaks, all of the radial luminosity profiles are relatively flat (accounting for the noise).

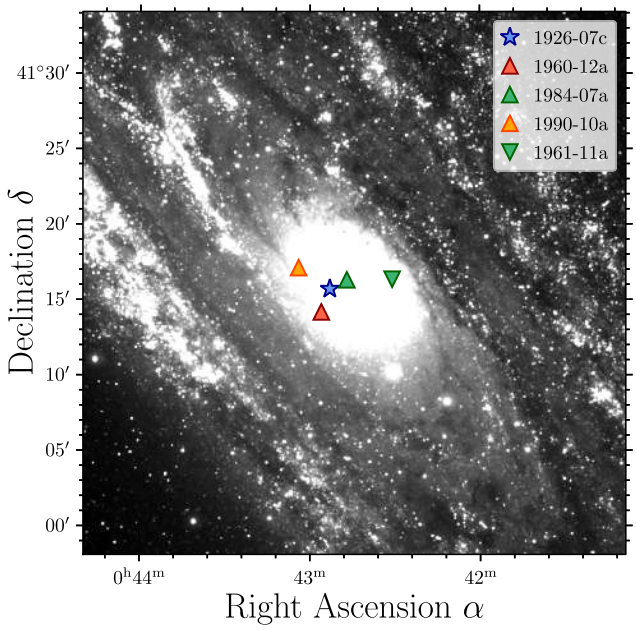

Figure 7. A zoom-in of the bulge of M 31 from the near-UV GALEX image shown in Fig. 2. Here, we show the locations of the five novae that we cannot analyse.

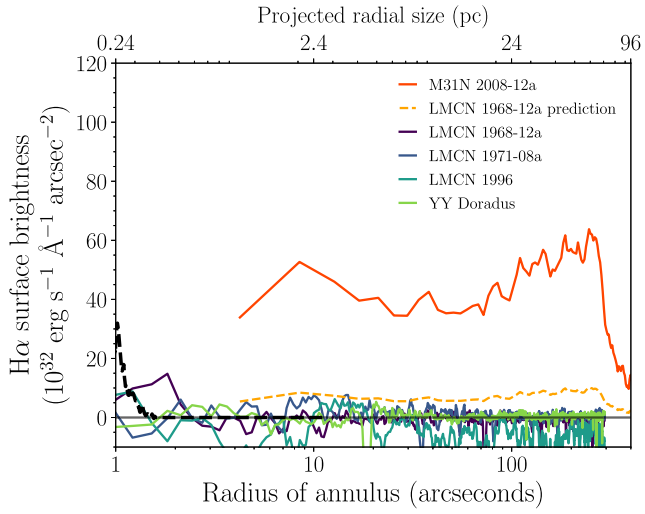

Figure 8. The Hα luminosity surface brightness of the surroundings of four novae in the LMC out to ∼295 arcsec (with a projected size of ∼71 pc at a distance of the LMC). This is emission determined from annular photometry after continuum subtraction and pixel masking of the bright sources in the images. As in Figs 5 and 6, we show the PSF for the FTS data (black dashed line). For comparison, we also include the 12a NSR Hα emission (from Fig. 5; the red line) but scaled to the distance of the LMC. The orange dashed line is a first-order approximation of the NSR emission profile for LMCN 1968–12a (see Section 4.2.1).

4.1.3 [O III] *luminosity*

As seen in the LGGS imaging, there is a total absence of [O III] from the NSR surrounding M31N 2008–12a, and so we find that this is the case when we quantify the emission; a very noisy luminosity profile averaging zero. The fourteen recurrent novae which we were able to analyse all show the same lack of extended [O III] emission

(consistent with noisy data averaging zero) therefore we have chosen to exclude the [O III] luminosity radial profile.

4.2 LMC

The surroundings of the four RNe shown in the continuum subtracted images (Figs A20–A23) do not unveil any type of structure centred on the central nova. This absence of extended emission is reflected in the results of the annular photometry analysis described in Section 3 and shown in Fig. 8.

4.2.1 H α luminosity

The lack of a discernible structure reminiscent of an NSR surrounding any of the four RNe in the LMC is quantified in Fig. 8. While noisy, each of the radial luminosity profiles are consistent with zero emission.

The only exception to the flat (noisy) profiles is the bump between ∼1 and 2.5 arcsec associated with LMCN 1968–12a. The point spread function for the FTS data is much smaller (see the black dashed line in Fig. 8) than in the LGGS data so may not necessarily be the reason behind the small peak. By inspection, within the continuum subtracted FTS H α image containing LMCN 1968–12a, the nova is located between two other stars therefore this apparent bump is likely to be contributions from the residuals of these two sources. The residuals are then likely to be compounded at these small radii, whereby the smallest apertures applied are more sensitive to (potentially extreme) pixel-to-pixel fluctuations.

In Fig. 8, we show the H α emission for the M 31 2008–12a NSR but as it would appear if the nova was in the LMC and, clearly, this NSR would be detectable in our data. As the NSR for LMCN 1968–12a is predicted to be approximately the same size as the NSR surrounding M 31 2008–12a, we have scaled the M 31 2008–12a NSR emission to match the difference in predicted flux for both NSRs (from Table 1) as a first-order approximation for the NSR emission profile of LMCN 1968–12a. This is shown as the orange dashed line in Fig. 8 and demonstrates that, given the LMC H α background and the extent of the FTS data, this NSR would be within the noise and therefore not detectable within our FTS data.

4.2.2 [O III] luminosity

In a same way that the LGGS [O III] imaging had no trace of extended emission around any RNe in M 31 (including 2008–12a as expected), the FTS [O III] imaging is also devoid of emission around the four RNe in the LMC. As such, the [O III] luminosity radial profiles for the four RNe quantified this absence with a noise profile consistent with zero flux. Therefore, we again omit this.

4.2.3 Recovered supernova remnant – MCSNR J0514−6840

In the south-west portion of the 10.5 arcmin × 10.5 arcmin FTS field centred on LMCN 1996, we do see extended H α emission from a known supernova remnant – MCSNR J0514−6840 (for example see fig. 3 in Maggi et al. 2014) – in the form of a shell, which we show in Fig. 9. Likewise, we see the supernova remnant shell, albeit with a different shape in our [O III] imaging of the same field (also shown in Fig. 9). In the H α image, the nearest edge of MCSNR J0514−6840 is approximately 3.9 arcmin from the location of the nova.

While not relevant to the objectives of our study, the detection of this supernova remnant in the LMC does illustrate the suitability of our data. It also demonstrates the requirement for [O III] imaging to differentiate NSRs from similar-looking astrophysical phenomena such as supernova remnants.

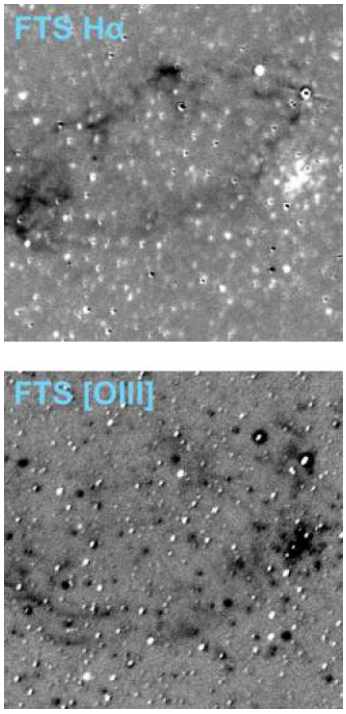

Figure 9. A 2.6 arcmin × 2.6 arcmin region of FTS data showing the supernova remnant MCSNR J0514−6840. It was found in the same FTS field of view as the RNe LMCN 1996 however note that the location of this nova is not within the above images. Top: FTS H α image. Bottom: FTS [O III] image.

4.3 When would the 12a NSR have been missed?

As can be seen clearly in Fig. 5 and Fig. A1, the NSR surrounding M 31N 2008–12a is well recovered in LGGS images. However, we will now look at how much fainter the structure associated with 12a would have to have been for it to have been missed; this could be analogous to the lack of emission seen around the other systems.

We explored this idea by taking the continuum-subtracted LGGS image containing the NSR surrounding 12a and setting the instrumental magnitude of the background to be the zero-point. We then added artificial noise to the image using the IRAF package `mknoise`, taking account of the change in magnitude of the background, until the NSR was no longer visible. By artificially brightening the background, we can determine how many magnitudes fainter the 12a NSR would have to be to evade discovery.

The outcome of this test can be seen in the left panels of Fig. 10. In the top left panel, we simply show the 1 arcmin × 1 arcmin region surrounding 12a (as in Fig. A1). The other eleven panels show the same region but with increasing levels of added Poisson noise to represent worsening signal to noise alongside the brightening of the background.

The bottom right panel of Fig. 10 shows the surroundings of 12a with 1.25 mag of noise added to the image (analogous to the remnant being 1.25 mag fainter). This reflects the difference in luminosity between the 12a NSR and the next brightest predicted NSR associated with M 31N 2017–01e (see Table 1). As can be seen, the 12a NSR is difficult to detect once the background has

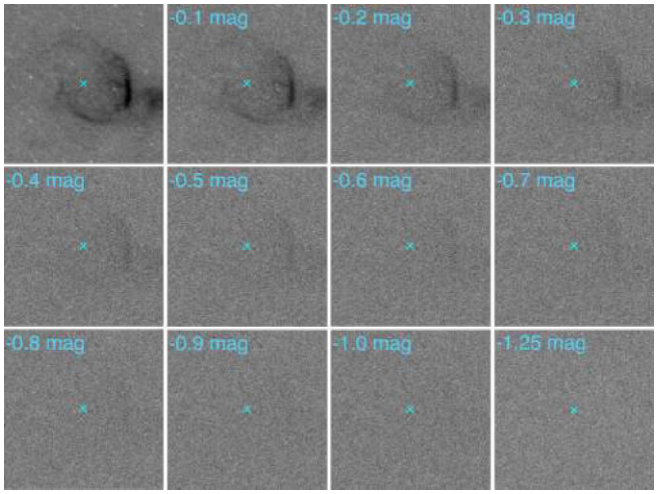

Figure 10. Adding artificial noise to the region where the NSR surrounding 12a is located. Left: Each panel shows the 1 arcmin × 1 arcmin region surrounding 12a with the level of noise added. The top left panel is the continuum-subtracted LGGS of the 12a NSR (no artificial noise added).

brightened by approximately one magnitude: this is equivalent to the remnant surrounding 12a not being detected if it were one magnitude fainter. Therefore, the brightest NSR in M 31 (around 12a) is only on the cusp of visibility. Furthermore, the 2017–01e NSR (and other NSRs in M 31) should not be detectable in LGGS data.

5 DISCUSSION

We applied our method of annular photometry to nineteen of the twenty-four known RNe in M 31 and the LMC (five M 31 RNe are located too close the bulge of that galaxy for suitable analysis). From the surroundings of these nineteen novae, we only recovered the known nova super-remnant associated with M 31N 2008–12a. The environs of the other RNe displayed a distance lack of extended emission across the narrow-band filters we investigated, even when co-adding the images.

One possible explanation of this NSR dearth could be related to the evolutionary phase of each system. As shown in Section 2.4, NSRs will be brightest when the responsible nova is at an extreme stage of its evolution. In other words, systems with the most massive (carbon–oxygen) WDs and highest accretion rates (as is the case with 12a), and therefore the shortest recurrence periods, are likely to host the brightest NSRs. Yet, from simulations (Healy-Kalesh et al. 2023a), even the RN with the next shortest recurrence period (∼2.5 yr for M 31N 2017–01e) is predicted to have approximately one-quarter of the Hα flux as the equivalent simulation with a one-year recurrence period (see the cyan line in Fig. 4). Therefore, the NSRs associated with all of the other RNe in M 31 and the LMC will simply be intrinsically fainter and thus more difficult to detect (as we explored in Section 4.3).

Another potential reason behind the absence of NSRs could be the local ISM density. Healy-Kalesh et al. (2023a) illustrated that the ISM density has a significant influence on the size of the evolving NSR. As such, a very low ISM density environment would permit the growth of a substantially large remnant. As with a longer recurrence period, this would result in an intrinsically fainter NSR.

An additional possibility for the lack of other NSRs in M 31 and the LMC may relate to the initial mass of the WD. It was demonstrated in Healy-Kalesh et al. (2023a) that the initial mass of the WD has a lesser impact on NSR growth in comparison to other system parameters (e.g. accretion rate). However, this small influence applies to WDs with initial masses that sit in the carbon-oxygen (CO) regime, whereby early in their evolution, the WDs are not massive enough to power rapidly recurring novae (and so *are* able to grow a large dynamical NSR over many eruptions; Healy-Kalesh et al. 2023a). On the other hand, if the RN originates from a WD initially formed as an ONe WD, as may be the case for a large number of RNe we have considered in this work, then it will have a short recurrence period from birth and consequently will not have been able to grow a large dynamical remnant. This smaller NSR size will thus hamper efforts of detection.

Lastly, we are considering that NSRs exist around all other RNe and so are proposing the reasoning behind not detecting these structures. But we might not be able to observe a 12a-like NSR around the other systems in M 31 and the LMC because these other novae do not host an NSR. While the simplest explanation for the lack of other remnants, it does not provide a satisfactory narrative in light of the NSRs around 12a and KT Eri being so prominent. Specifically, Darnley et al. (2019) used hydrodynamical simulations to show that a structure reminiscent of the 12a NSR could be grown from frequent nova eruptions; this prediction was reinforced for 12a by Healy-Kalesh et al. (2023a), shown to apply to all RNe systems (whether the WD was growing or shrinking) and recently demonstrated for KT Eri (Healy-Kalesh et al. 2023b). Simulations correctly predicting the existence of the 12a NSR then not applying to other RNe is dubious – this lends support to the NSRs in M 31 and the LMC being too faint (or too small) to currently detect.

6 CONCLUSIONS

In this paper, we have conducted the first ever survey for nova super-remnants within M 31 using the imaging data collected as part of the Local Group Galaxies Survey. Additionally, we present our targeted search for nova super-remnants within the LMC using data collected with the FTS. Here, we summarize the key results of the paper:

(i) The prototypical nova super-remnant, surrounding the rapidly recurring nova M 31N 2008–12a, is recovered in the LGGS narrow-band Hα and [S II] images and absent in the [O III], as expected.

(ii) There is no Hα or [S II] emission apparent around the other fourteen recurrent novae in M 31 which we are able quantify with annular photometry (five novae were omitted from our analysis due to close proximity with the bulge of M 31).

(iii) There is no Hα emission apparent around the four recurrent novae in the LMC which we are able to quantify with annular photometry.

(iv) The 12a NSR would likely to have been missed if it were approximately one magnitude fainter.

(v) The distinct lack of an NSR around the RNe in M 31 and the LMC could possibly be explained by longer recurrence periods or very low-density ISM contributing to their intrinsic faintness.

(vi) The dearth of NSRs may also be resolved through considering that RNe with ONe WDs have a short recurrence period at birth thus will not host a large NSR, complicating their detection.

(vii) Alternatively, NSRs around the other RNe we considered may not exist and the 12a NSR is an extremely rare phenomenon, however this seems to be contrived based on the recent discovery of an NSR surrounding KT Eri.

Regardless of the underlying reason, we were not able to recover any other NSR in the vicinity of the majority of RNe in M 31 and the

RNe in the LMC. Moving forward, deeper narrow-band observations should be focused on the surroundings of the novae with the shortest recurrence periods.

ACKNOWLEDGEMENTS

The authors would like to thank our anonymous referee for their time spent reviewing our manuscript. MWH-K acknowledges a PDRA position funded by the UK Science and Technology Facilities Council (STFC). MWH-K and MJD receive funding from STFC grant number ST/S505559/1. MMS acknowledges the support of NSF award 2108234. This work was only possible with data from the Local Group Galaxy Survey. We would also like to thank Emily Manne-Nicholas for her generous help in coordinating our FTS observations for the LMC RNe data. This work has made use of data from the European Space Agency (ESA) mission *Gaia* (https://www.cosmos.esa.int/gaia), processed by the *Gaia* Data Processing and Analysis Consortium (DPAC, https://www.cosmos.esa.int/web/gaia/dpac/consortium). Funding for the DPAC was provided by national institutions, in particular the institutions participating in the *Gaia* Multilateral Agreement.

DATA AVAILABILITY

All data/image analysis was carried out using IRAF (Tody 1986, 1993), DAOPHOT (Stetson 1987), `astropy` (v4.0; The Astropy Collaboration et al. 2018), and `photutils` (v0.7.2; Bradley et al. 2019). The analysis in this work made use of the Python libraries: NUMPY (Harris et al. 2020) and MATPLOTLIB (Hunter 2007).

REFERENCES

Azimlu M., Marciniak R., Barmby P., 2011, AJ, 142, 139
Bode M. F., O'Brien T. J., Simpson M., 2004, ApJ, 600, L63
Bode M. F. et al., 2016, ApJ, 818, 145
Bond H. E., Walter F., Espinoza J., Gonzalez D., Pasten A., Green D. W. E., 2004, Int. Astron. Union Circ., 8424, 1
Bradley L. et al., 2019, Astropy/photutils: v0.7.2.
Darnley M. J., 2021, in Proc. Sci., The Golden Age of Cataclysmic Variables and Related Objects V (GOLDEN2019). SISSA, Trieste, PoS#368
Darnley M. J., Henze M., 2020, Adv. Space Res., 66, 1147
Darnley M. J., Williams S. C., 2021, Astron. Telegram, 14750, 1
Darnley M. J. et al., 2006, MNRAS, 369, 257
Darnley M. J., Williams S. C., Bode M. F., Henze M., Ness J.-U., Shafter A. W., Hornoch K., Votruba V., 2014, A&A, 563, L9
Darnley M. J. et al., 2015, A&A, 580, A45
Darnley M. J. et al., 2016, ApJ, 833, 149
Darnley M. J. et al., 2017, ApJ, 849, 96
Darnley M. J. et al., 2019, Nature, 565, 460
Gaia Collaboration, 2016, A&A, 595, A1
Gaia Collaboration, 2018, A&A, 616, A1
Hachisu I., Kato M., Nomoto K., Umeda H., 1999a, ApJ, 519, 314
Hachisu I., Kato M., Nomoto K., 1999b, ApJ, 522, 487
Harman D. J., O'Brien T. J., 2003, MNRAS, 344, 1219
Harris C. R. et al., 2020, Nature, 585, 357
Harvey E., Redman M. P., Boumis P., Akras S., 2016, A&A, 595, A64
Harvey E. J. et al., 2020, MNRAS, 499, 2959
Healy-Kalesh M. W., Darnley M. J., Harvey É. J., Copperwheat C. M., James P. A., Andersson T., Henze M., O'Brien T. J., 2023a, MNRAS, 521, 3004
Healy-Kalesh M. W., Darnley M. J., Shara M. M., Lanzetta K. M., Garland J. T., Gromoll S., 2023b, MNRAS, preprint (arXiv:2310.17258)
Hillebrandt W., Niemeyer J. C., 2000, ARA&A, 38, 191
Hillman Y., Prialnik D., Kovetz A., Shara M. M., 2015, MNRAS, 446, 1924
Hillman Y., Prialnik D., Kovetz A., Shara M. M., 2016, ApJ, 819, 168
Hunter J. D., 2007, Comput. Sci. Eng., 9, 90
Kato M., Saio H., Hachisu I., 2015, ApJ, 808, 52
Kuin N. P. M. et al., 2020, MNRAS, 491, 655
Lanzetta K. M., Gromoll S., Shara M. M., Berg S., Valls-Gabaud D., Walter F. M., Webb J. K., 2023, PASP, 135, 015002
Maggi P. et al., 2014, A&A, 561, A76
Mason E., Ederoclite A., Stefanon M., dall T. H., Della Valle M., 2004, Int. Astron. Union Circ., 8424, 2
Massey P., Olsen K. A. G., Hodge P. W., Strong S. B., Jacoby G. H., Schlingman W., Smith R. C., 2006, AJ, 131, 2478
Massey P., McNeill R. T., Olsen K. A. G., Hodge P. W., Blaha C., Jacoby G. H., Smith R. C., Strong S. B., 2007, AJ, 134, 2474
Mellinger A., 2009, PASP, 121, 1180
Mróz P., Udalski A., 2018, Astron. Telegram, 11384, 1
Nishiyama K., Kabashima F., 2008, Int. Astron. Union Circ., 8938
Pagnotta A., Schaefer B. E., 2014, ApJ, 788, 164
Pietrzyński G. et al., 2019, Nature, 567, 200
Prialnik D., Shara M. M., Shaviv G., 1978, A&A, 62, 339
Schaefer B. E., 2010, ApJS, 187, 275
Schaefer B. E., Pagnotta A., Shara M. M., 2010, ApJ, 708, 381
Schaefer B. E., Walter F. M., Hounsell R., Hillman Y., 2022, MNRAS, 517, 3864
Shafter A. W., 2019, Extragalactic Novae: A Historical Perspective. IOP Publishing, Bristol, UK
Shafter A. W. et al., 2015, ApJS, 216, 34
Shafter A. W. et al., 2022a, Res. Notes Am. Astron. Soc., 6, 214
Shafter A. W., Taguchi K., Zhao J., Hornoch K., 2022b, Res. Notes Am. Astron. Soc., 6, 241
Shafter A. W. et al., 2023, Astron. Telegram, 16354, 1
Shara M. M., Zurek D. R., Williams R. E., Prialnik D., Gilmozzi R., Moffat A. F. J., 1997, AJ, 114, 258
Shara M. M. et al., 2007, Nature, 446, 159
Shara M. M., Mizusawa T., Wehinger P., Zurek D., Martin C. D., Neill J. D., Forster K., Seibert M., 2012, ApJ, 758, 121
Shara M. M. et al., 2015, ApJ, 805, 148
Shara M. M. et al., 2023, preprint (arXiv:2310.17055)
Stanek K. Z., Garnavich P. M., 1998, ApJ, 503, L131
Starrfield S., Truran J. W., Sparks W. M., Kutter G. S., 1972, ApJ, 176, 169
Stetson P. B., 1987, PASP, 99, 191
Sun G., Xu J., Zhang M., Zhou W., Zhao J., Ruan J., Gao X., 2023, Astron. Telegram, 16361, 1
The Astropy Collaboration, 2018, AJ, 156, 123
Tody D., 1986, in Crawford D. L., ed., Proc. SPIE Conf. Ser. Vol. 627, Instrumentation in Astronomy VI. SPIE, Bellingham, p. 733
Tody D., 1993, in Hanisch R. J., Brissenden R. J. V., Barnes J., eds, ASP Conf. Ser. Vol. 52, Astronomical Data Analysis Software and Systems II. Astron. Soc. Pac., San Francisco, p. 173
Toraskar J., Mac Low M.-M., Shara M. M., Zurek D. R., 2013, ApJ, 768, 48
Walterbos R. A. M., Braun R., 1992, A&AS, 92, 625
Warner B., 1995, Cataclysmic Variable Stars, Cambridge Astrophysics Series. Cambridge Univ. Press, Cambridge
Weiler M., 2018, A&A, 617, A138
Whelan J., Iben I.,, Jr, 1973, ApJ, 186, 1007
Williams S. C., Darnley M. J., 2017, Astron. Telegram, 10042, 1
Williams R. E., Woolf N. J., Hege E. K., Moore R. L., Kopriva D. A., 1978, ApJ, 224, 171
Xu J. et al., 2023, Transient Name Server Discovery Report (TR) 2023 ID #3081
Yaron O., Prialnik D., Shara M. M., Kovetz A., 2005, ApJ, 623, 398

APPENDIX: SURROUNDINGS OF RECURRENT NOVAE

Here, we provide the LGGS (Massey et al. 2007) narrow-band imaging (Hα, [S II] and [O III]) of the 1 arcmin × 1 arcmin region surrounding nineteen of the twenty recurrent novae within M 31 (the surroundings of M 31N 1984–07a have been omitted due to

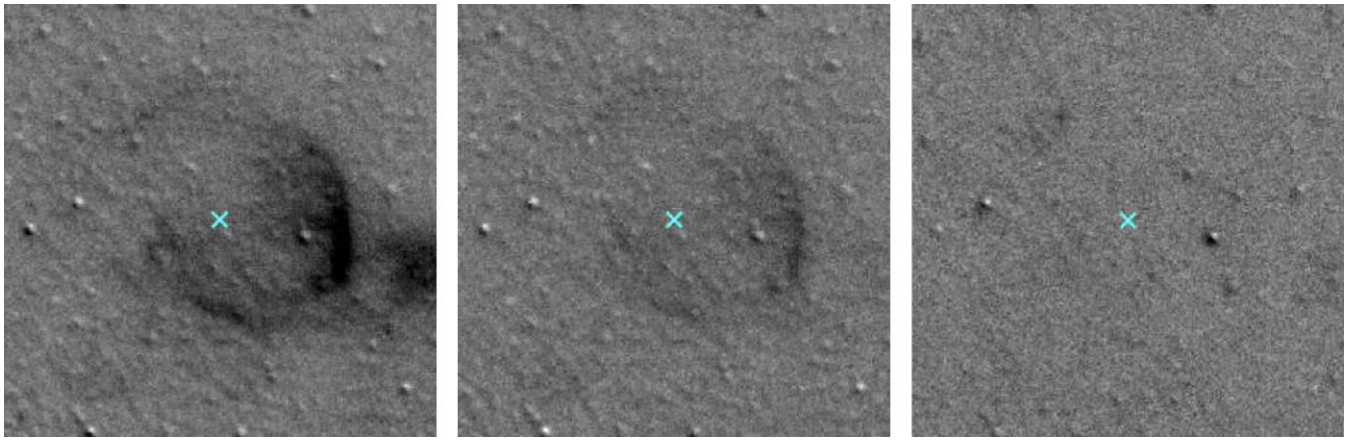

Figure A1. – M 31N 2008–12a. The location of the nova (in field 3) is indicated by the blue cross. Left: continuum subtracted LGGS H α. Middle: continuum subtracted LGGS [S II]. Right: continuum subtracted LGGS [O III].

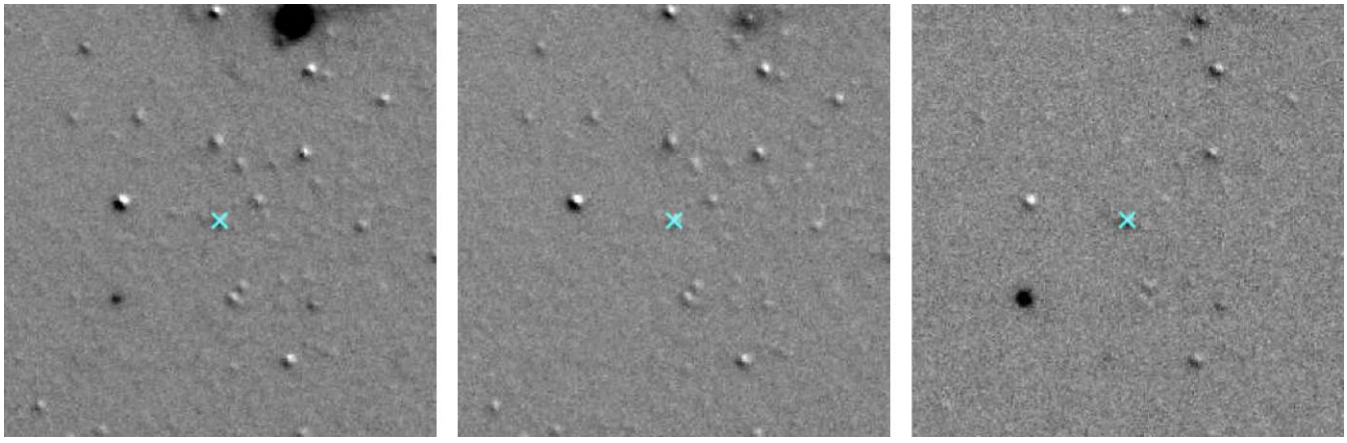

Figure A2. – M 31N 2017–01e. The location of the nova (in field 3) is indicated by the blue cross. Left: continuum subtracted LGGS H α. Middle: continuum subtracted LGGS [S II]. Right: continuum subtracted LGGS [O III].

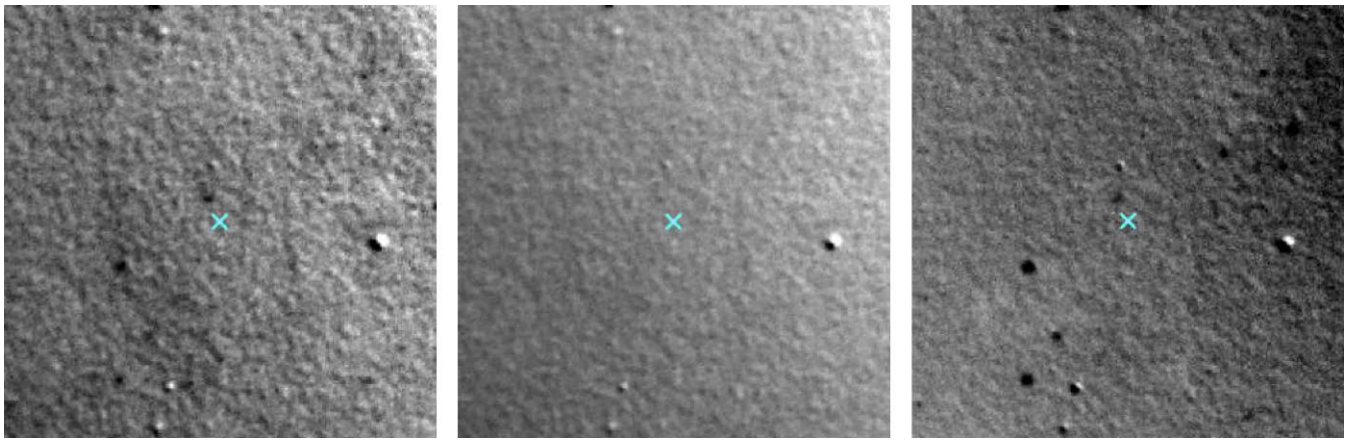

Figure A3. – M 31N 1926–07c. The location of the nova (in field 6) is indicated by the blue cross. Left: continuum subtracted LGGS H α. Middle: continuum subtracted LGGS [S II]. Right: continuum subtracted LGGS [O III].

its extreme proximity to the centre of M 31). We also provide Faulkes Telescope South narrow-band imaging (H α and [O III]) of the 1.5 arcmin $\times$ 1.5 arcmin region surrounding each of the four recurrent novae within the LMC.

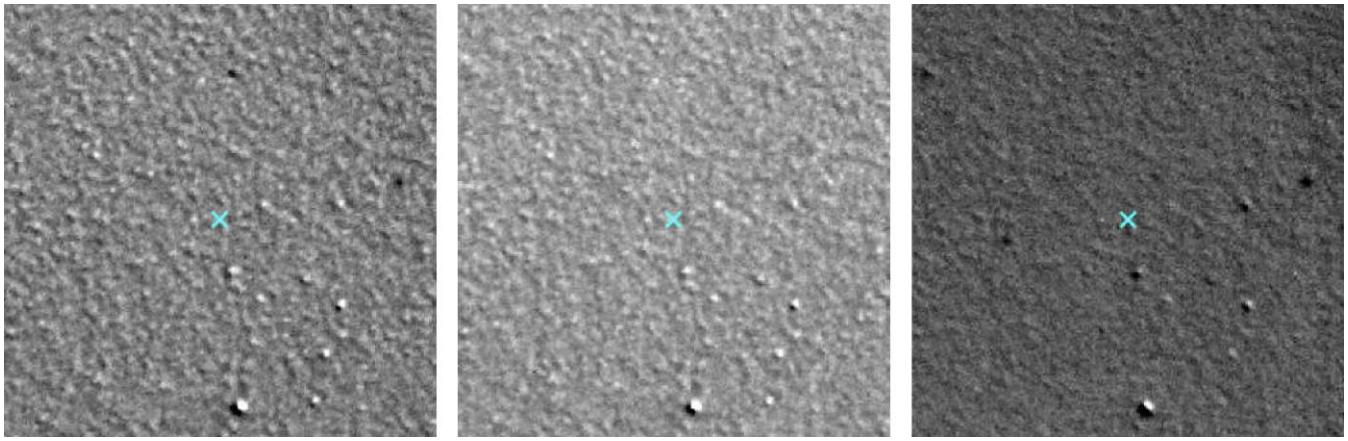

Figure A4. – M 31N 1997–11k. The location of the nova (in field 6) is indicated by the blue cross. Left: continuum subtracted LGGS H α. Middle: continuum subtracted LGGS [S II]. Right: continuum subtracted LGGS [O III].

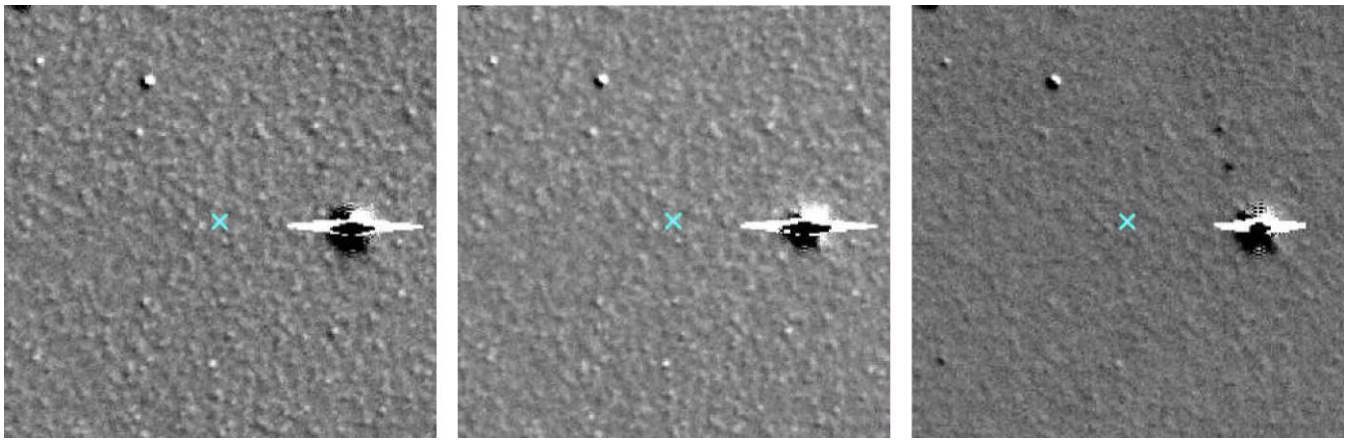

Figure A5. – M 31N 1963–09c. The location of the nova (in field 6) is indicated by the blue cross. Left: continuum subtracted LGGS H α. Middle: continuum subtracted LGGS [S II]. Right: continuum subtracted LGGS [O III].

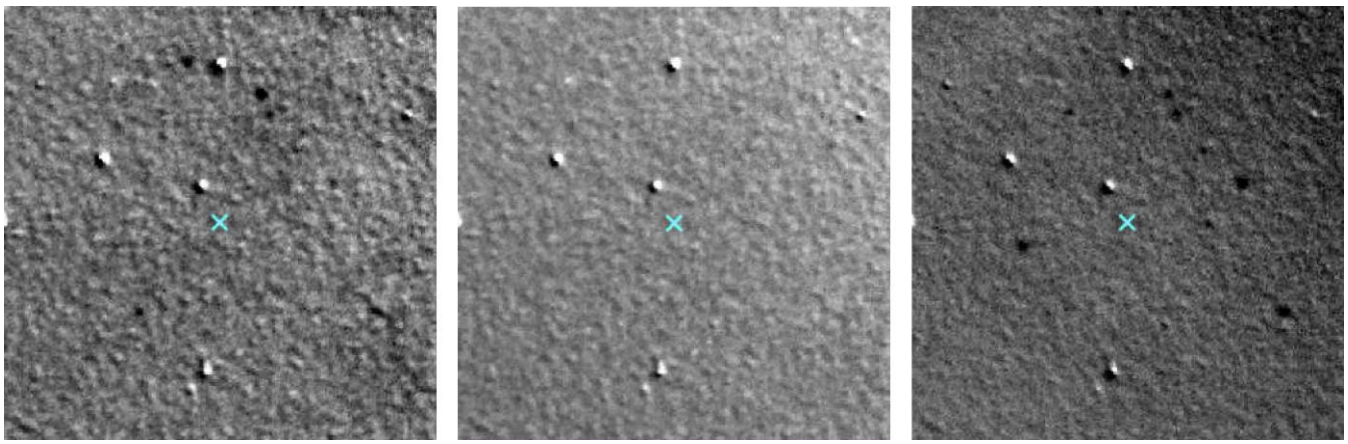

Figure A6. – M 31N 1960–12a. The location of the nova (in field 6) is indicated by the blue cross. Left: continuum subtracted LGGS H α. Middle: continuum subtracted LGGS [S II]. Right: continuum subtracted LGGS [O III].

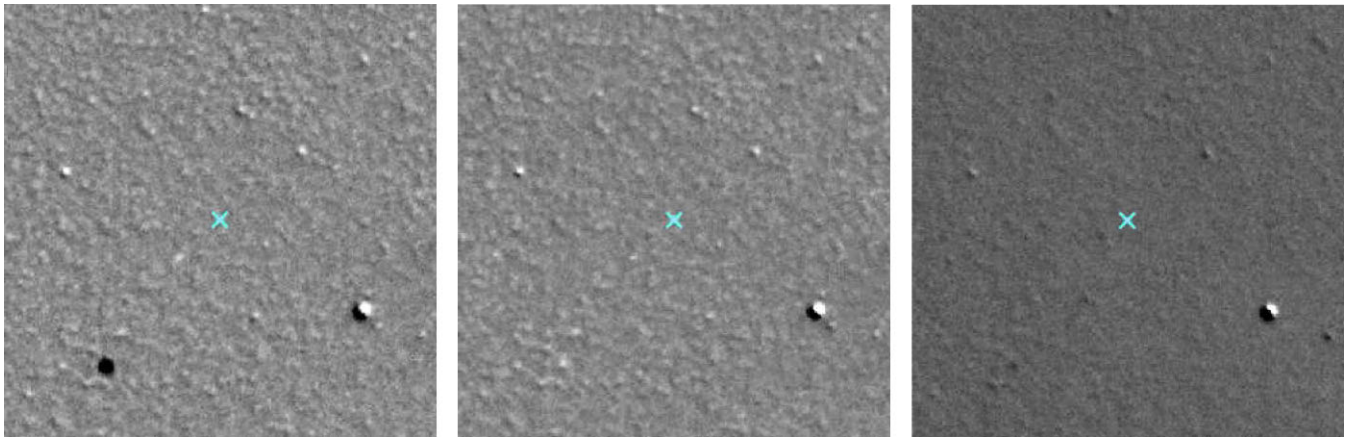

Figure A7. – M 31N 2006–11c. The location of the nova (in field 6) is indicated by the blue cross. Left: continuum subtracted LGGS H α. Middle: continuum subtracted LGGS [S II]. Right: continuum subtracted LGGS [O III].

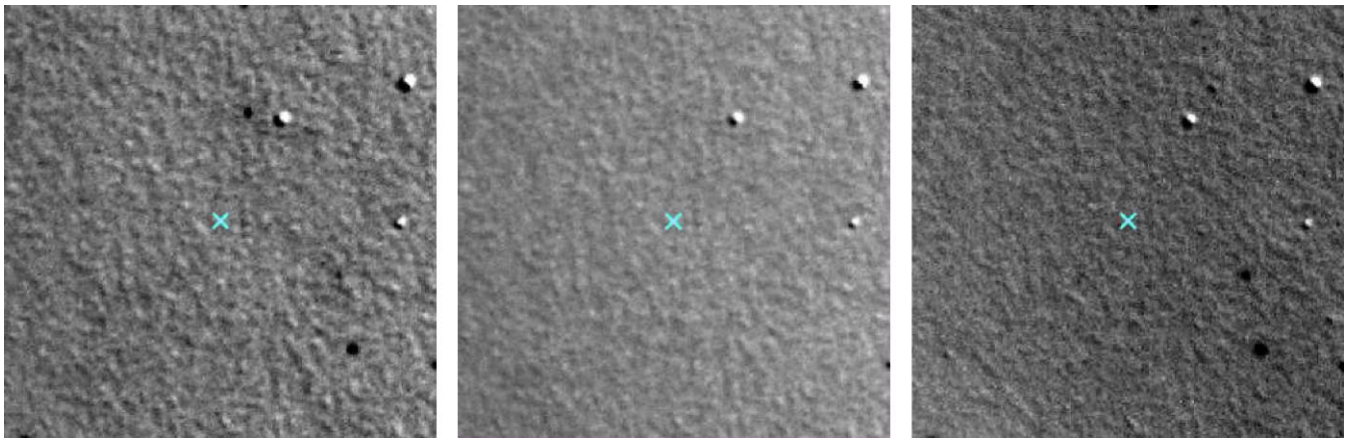

Figure A8. – M 31N 1990–10a. The location of the nova (in field 6) is indicated by the blue cross. Left: continuum subtracted LGGS H α. Middle: continuum subtracted LGGS [S II]. Right: continuum subtracted LGGS [O III].

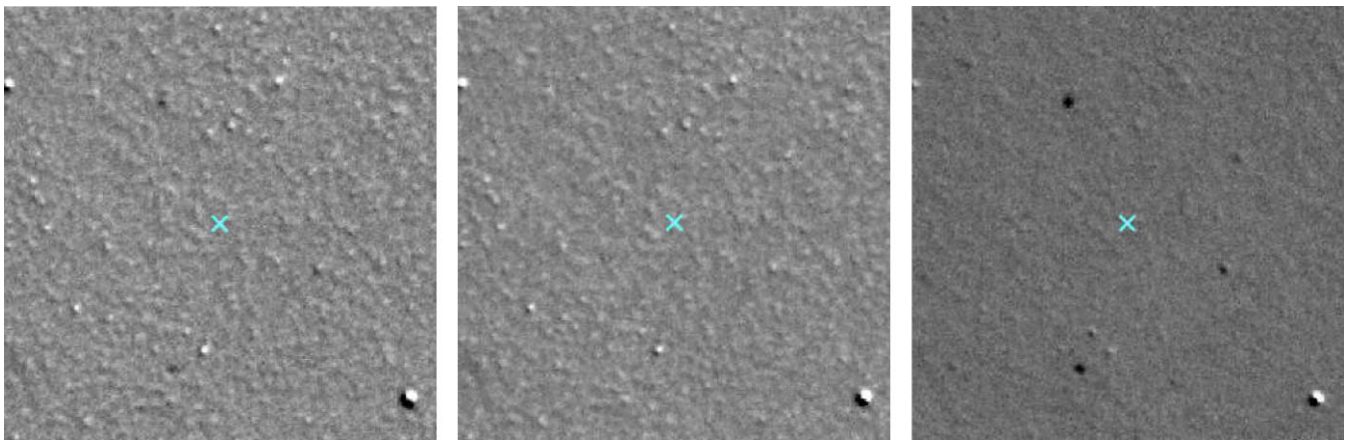

Figure A9. – M 31N 2007–11f. The location of the nova (in field 6) is indicated by the blue cross. Left: continuum subtracted LGGS H α. Middle: continuum subtracted LGGS [S II]. Right: continuum subtracted LGGS [O III].

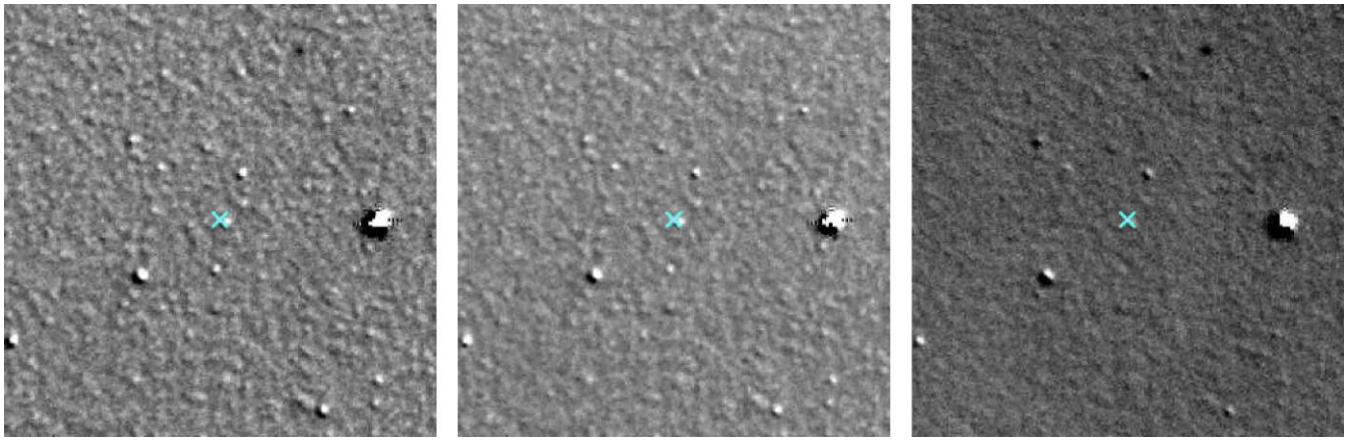

Figure A10. – M 31N 1923–12c. The location of the nova (in field 6) is indicated by the blue cross. Left: continuum subtracted LGGS H α. Middle: continuum subtracted LGGS [S II]. Right: continuum subtracted LGGS [O III].

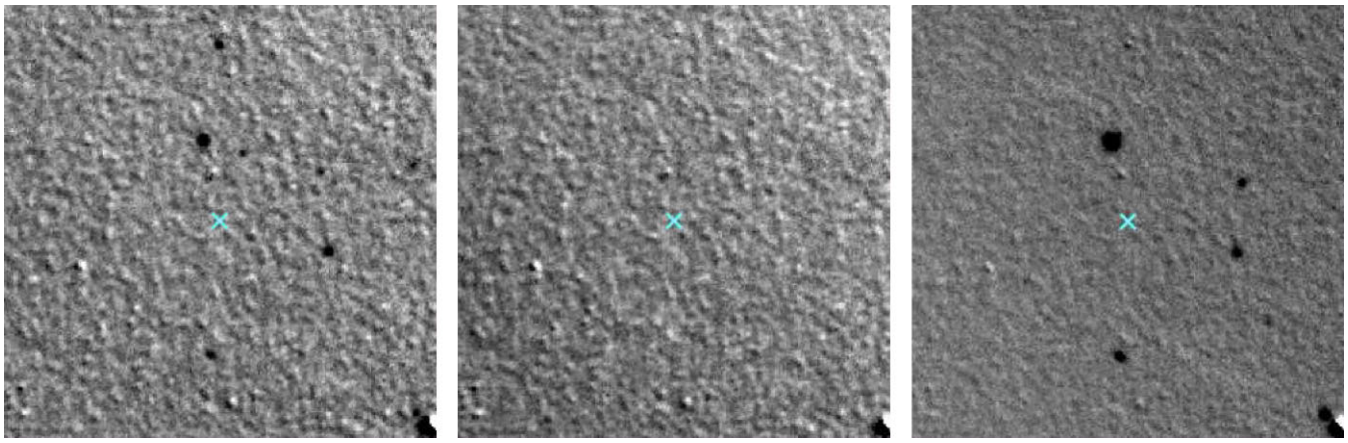

Figure A11. – M 31N 2013–10c. The location of the nova (in field 6) is indicated by the blue cross. Left: continuum subtracted LGGS H α. Middle: continuum subtracted LGGS [S II]. Right: continuum subtracted LGGS [O III].

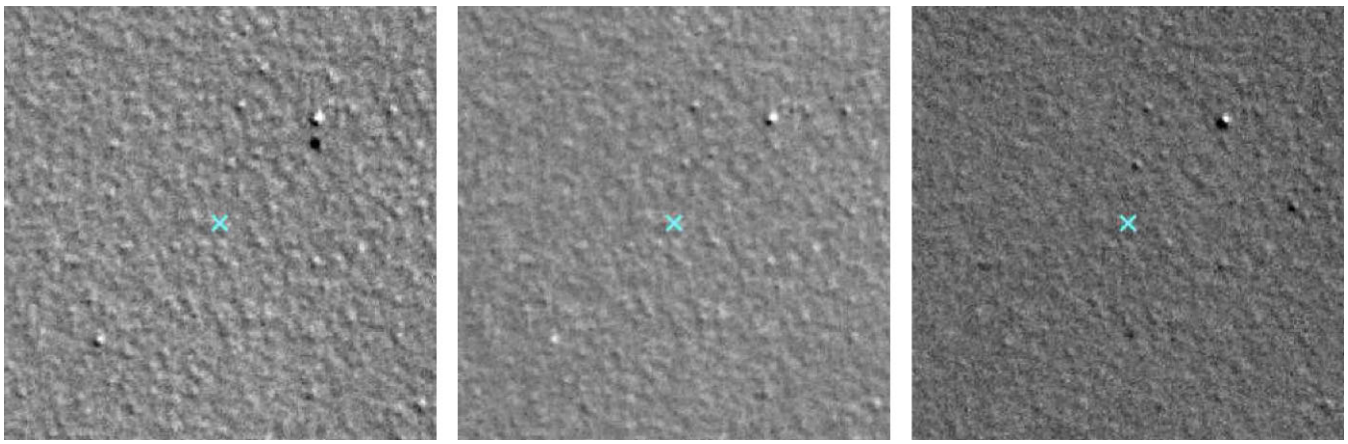

Figure A12. – M 31N 2007–10b. The location of the nova (in field 6) is indicated by the blue cross. Left: continuum subtracted LGGS H α. Middle: continuum subtracted LGGS [S II]. Right: continuum subtracted LGGS [O III].

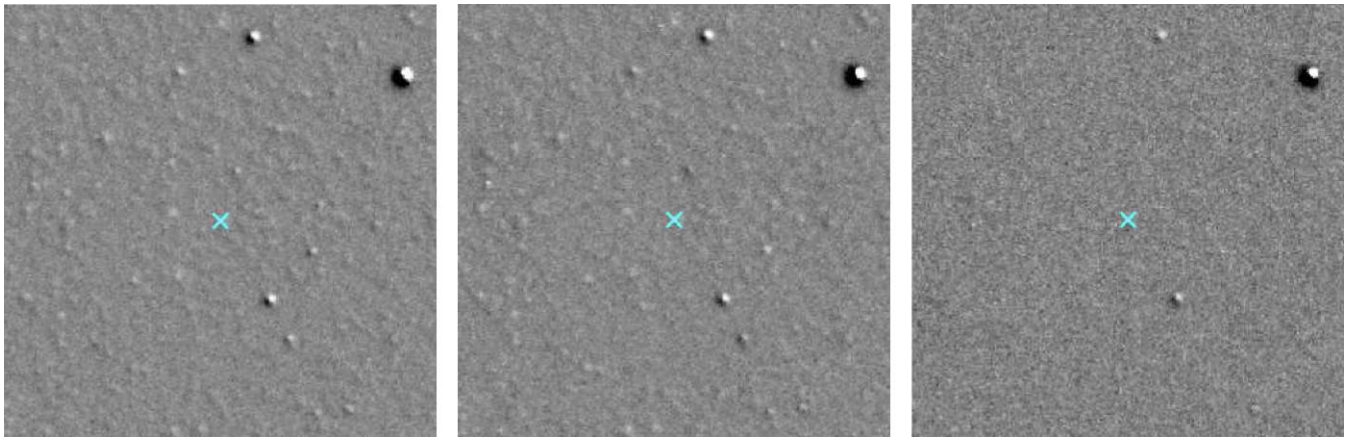

Figure A13. – M 31N 1982–08b. The location of the nova (in field 3) is indicated by the blue cross. Left: continuum subtracted LGGS H α. Middle: continuum subtracted LGGS [S II]. Right: continuum subtracted LGGS [O III].

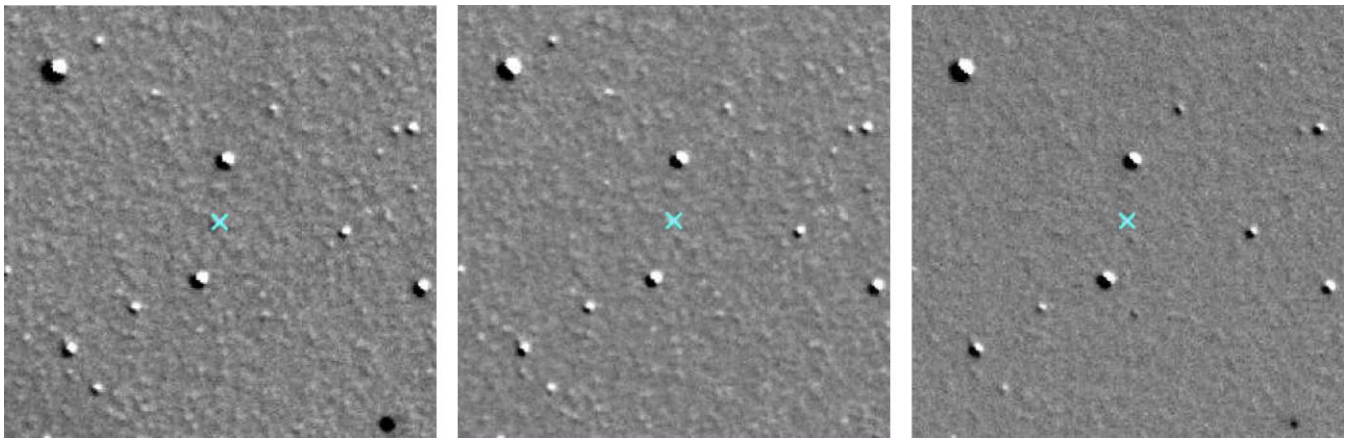

Figure A14. – M 31N 1945–09c. The location of the nova (in field 6) is indicated by the blue cross. Left: continuum subtracted LGGS H α. Middle: continuum subtracted LGGS [S II]. Right: continuum subtracted LGGS [O III].

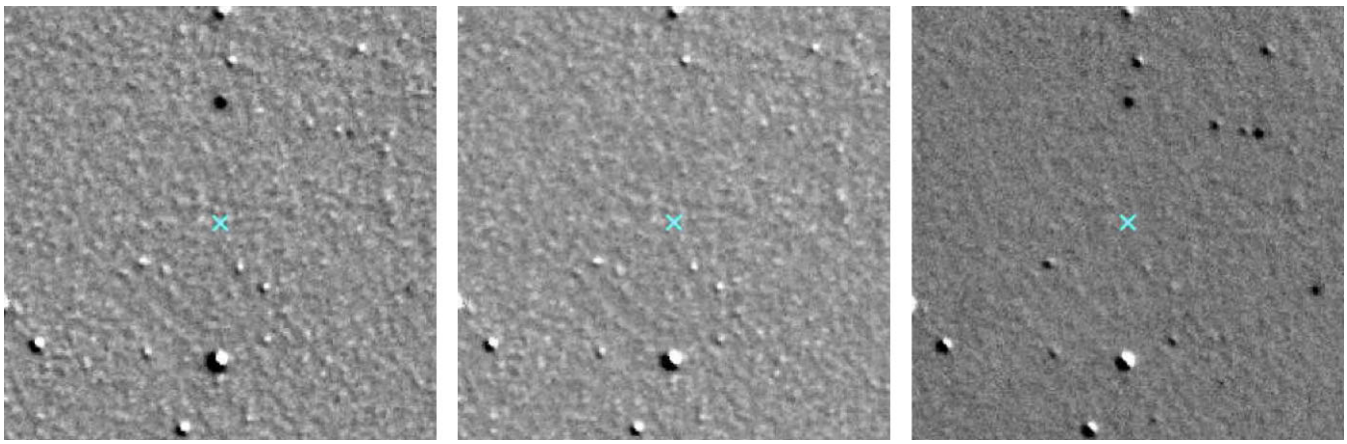

Figure A15. – M 31N 1926–06a. The location of the nova (in field 6) is indicated by the blue cross. Left: continuum subtracted LGGS H α. Middle: continuum subtracted LGGS [S II]. Right: continuum subtracted LGGS [O III].

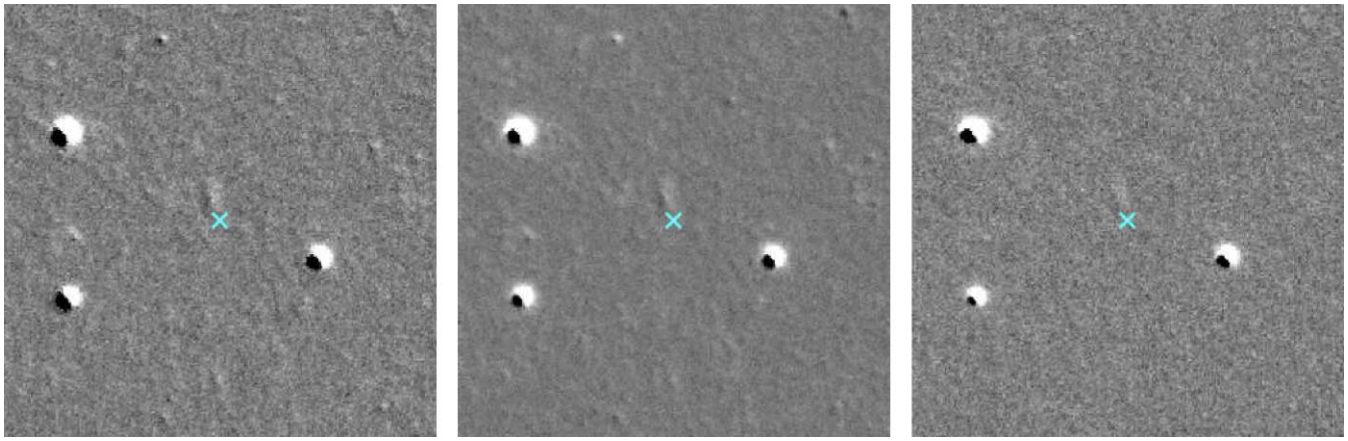

Figure A16. – M 31N 1966–09e. The location of the nova (in field 8) is indicated by the blue cross. Left: continuum subtracted LGGS H α. Middle: continuum subtracted LGGS [S II]. Right: continuum subtracted LGGS [O III].

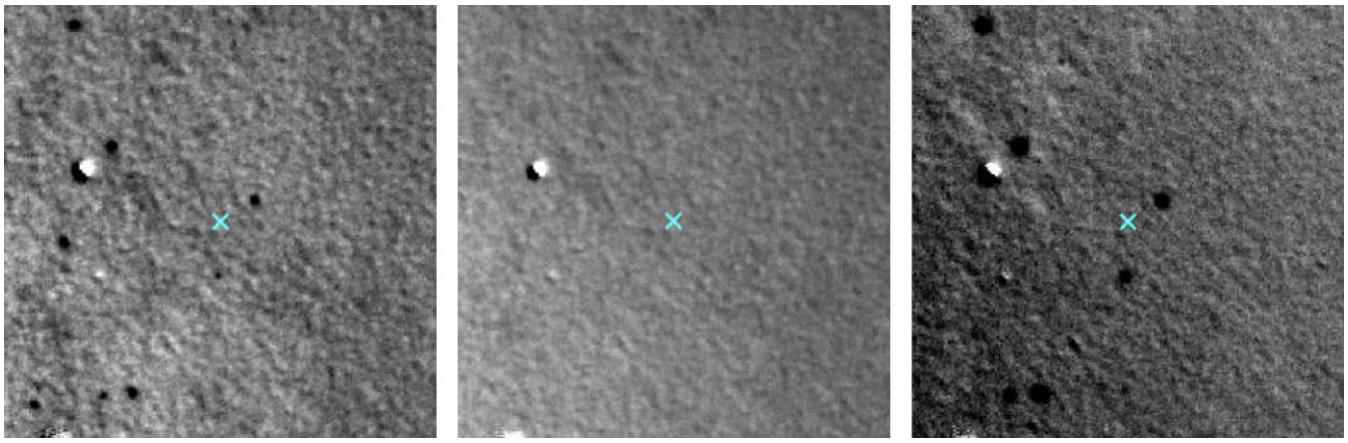

Figure A17. – M 31N 1961–11a. The location of the nova (in field 6) is indicated by the blue cross. Left: continuum subtracted LGGS H α. Middle: continuum subtracted LGGS [S II]. Right: continuum subtracted LGGS [O III].

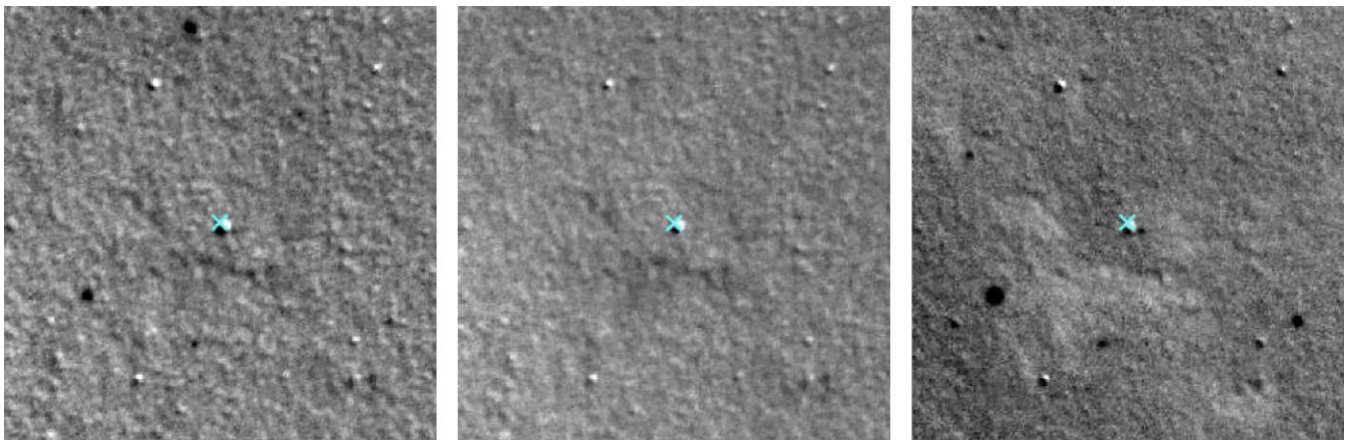

Figure A18. – M 31N 1953–09b. The location of the nova (in field 6) is indicated by the blue cross. Left: continuum subtracted LGGS H α. Middle: continuum subtracted LGGS [S II]. Right: continuum subtracted LGGS [O III].

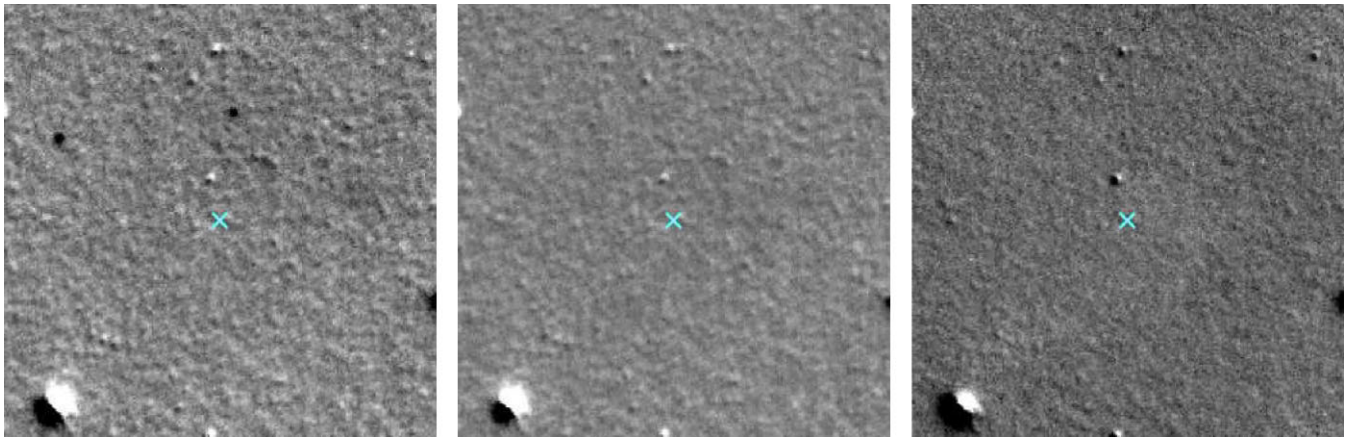

Figure A19. – M 31N 1919–09a. The location of the nova (in field 6) is indicated by the blue cross. Left: continuum subtracted LGGS Hα. Middle: continuum subtracted LGGS [S II]. Right: continuum subtracted LGGS [O III].

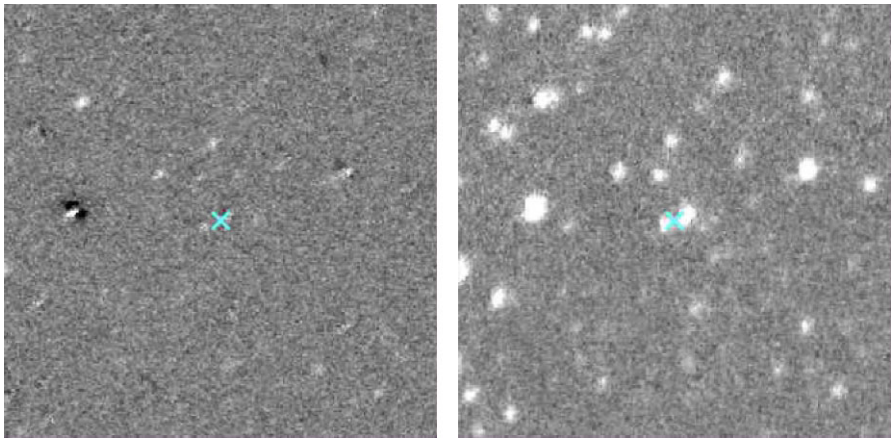

Figure A20. – LMCN 1968–12a. The location of the nova is indicated by the blue cross. Left: continuum subtracted FTS Hα. Right: continuum subtracted FTS [O III].

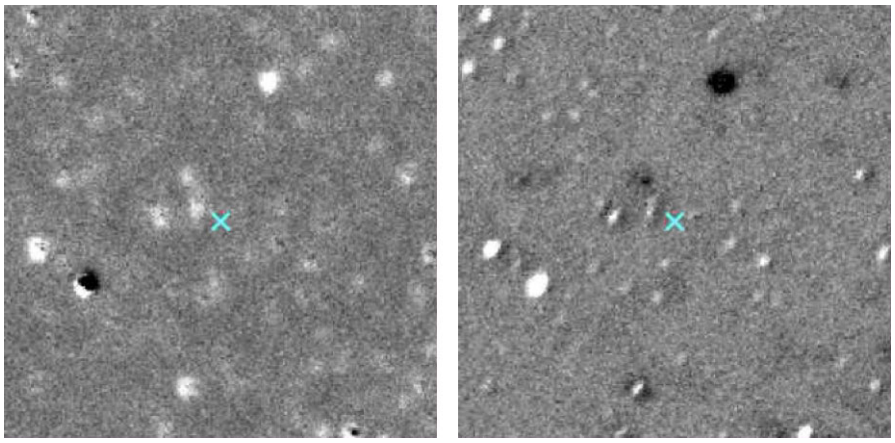

Figure A21. – LMCN 1996. The location of the nova is indicated by the blue cross. Left: continuum subtracted FTS Hα. Right: continuum subtracted FTS [O III].

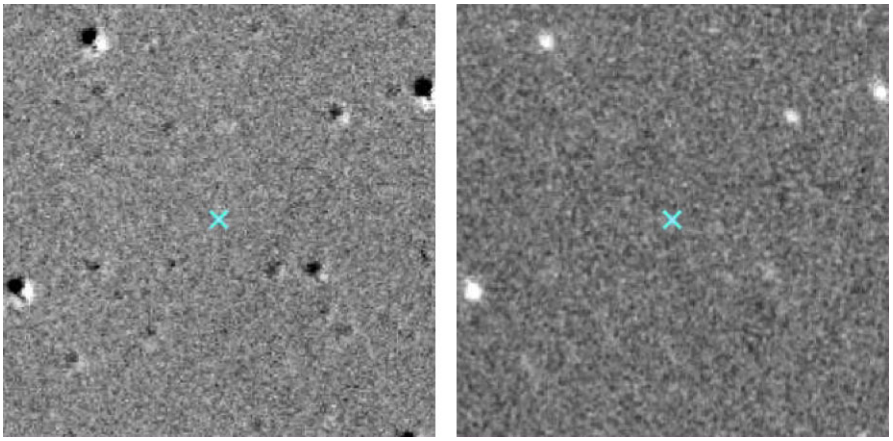

Figure A22. – LMCN 1971–08a. The location of the nova is indicated by the blue cross. Left: continuum subtracted FTS Hα. Right: continuum subtracted FTS [O III].

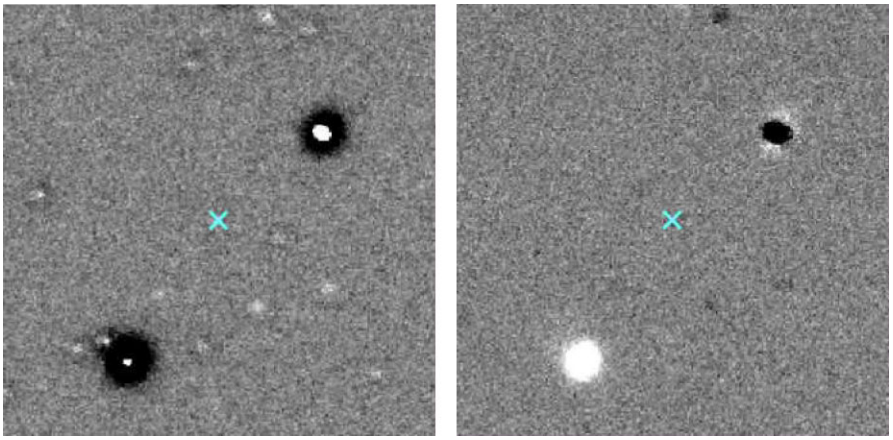

Figure A23. – YY Doradus. The location of the nova is indicated by the blue cross. Left: continuum subtracted FTS Hα. Right: continuum subtracted FTS [O III].

This paper has been typeset from a TEX/LATEX file prepared by the author.